Automatic classification of patients with Alzheimer's disease from structural MRI: a comparison of ten methods using the ADNI database

Rémi Cuingnet, Emilie Gerardin, Jérôme Tessieras, Guillaume Auzias, Stéphane Lehéricy, Marie-Odile Habert, Marie Chupin, Habib Benali, Olivier Colliot

Automatic classification of patients with Alzheimer's disease from structural MRI: a comparison of ten methods using the ADNI database

Rémi Cuingnet[1,2,3,4], MSc; Emilie Gérardin[1,2,3], MSc; Jérôme Tessieras[1,2,3], MSc; Guillaume Auzias[1,2,3], MSc; Stéphane Lehéricy[1,2,3,5], MD, PhD; Marie-Odile Habert[4,6], MD, PhD; Marie Chupin[1,2,3], PhD; Habib Benali[4], PhD; Olivier Colliot[1,2,3], PhD and the Alzheimer's Disease Neuroimaging Initiative*

[1]UPMC Université Paris 6, UMR 7225, UMR_S 975, Centre de Recherche de l'Institut du Cerveau et de la Moelle épinière (CRICM), Paris, F-75013, France
[2]CNRS, UMR 7225, CRICM, Paris, F-75013, France
[3]Inserm, UMR_S 975, CRICM, Paris, F-75013, France
[4]Inserm, UMR_S 678, LIF, Paris, F-75013, France
[5]Centre for NeuroImaging Research – CENIR, Department of Neuroradiology, Groupe hospitalier Pitié-Salpêtrière, Paris, F-75013, France
[6]AP-HP, Department of Nuclear Medicine, Groupe hospitalier Pitié-Salpêtrière, Paris, F-75013, France

Key words: Alzheimer's disease, AD, MCI, converter, prodromal, classification, magnetic resonance imaging, support vector machines,

Type of manuscript: Review

Correspondence to:
Rémi Cuingnet
CRICM – Equipe Cogimage (ex LENA)
Hôpital de la Pitié-Salpêtrière
47, boulevard de l'hôpital
75651 Paris Cedex 13
France
Phone: +33 1 42 17 85 24
e-mail: remi.cuingnet@gmail.com

* Data used in the preparation of this article were obtained from the Alzheimer's Disease Neuroimaging Initiative (ADNI) database (www.loni.ucla.edu/ADNI). As such, the investigators within the ADNI contributed to the design and implementation of ADNI and/or provided data but did not participate in analysis or writing of this report. ADNI investigators include (complete listing available at www.loni.ucla.edu/ADNI/Collaboration/ADNI Author ship list.pdf).

Abstract

Recently, several high dimensional classification methods have been proposed to automatically discriminate between patients with Alzheimer's disease (AD) or mild cognitive impairment (MCI) and elderly controls (CN) based on T1-weighted MRI. However, these methods were assessed on different populations, making it difficult to compare their performance. In this paper, we evaluated the performance of ten approaches (five voxel-based methods, three methods based on cortical thickness and two methods based on the hippocampus) using 509 subjects from the ADNI database. Three classification experiments were performed: CN *vs* AD, CN *vs* MCIc (MCI who had converted to AD within 18 months, MCI converters - MCIc) and MCIc *vs* MCInc (MCI who had not converted to AD within 18 months, MCI non-converters - MCInc). Data from 81 CN, 67 MCInc, 39 MCIc and 69 AD were used for training and hyperparameters optimization. The remaining independent samples of 81 CN, 67 MCInc, 37 MCIc and 68 AD were used to obtain an unbiased estimate of the performance of the methods. For AD *vs* CN, whole-brain methods (voxel-based or cortical thickness-based) achieved high accuracies (up to 81% sensitivity and 95% specificity). For the detection of prodromal AD (CN *vs* MCIc), the sensitivity was substantially lower. For the prediction of conversion, no classifier obtained significantly better results than chance. We also compared the results obtained using the DARTEL registration to that using SPM5 unified segmentation. DARTEL significantly improved six out of 20 classification experiments and led to lower results in only two cases. Overall, the use of feature selection did not improve the performance but substantially increased the computation times.

Introduction

Alzheimer's disease (AD) is the most frequent neurodegenerative dementia and a growing health problem. Definite diagnosis can only be made postmortem, and requires histopathological confirmation of amyloid plaques and neurofibrillary tangles. Early and accurate diagnosis of Alzheimer's Disease (AD) is not only challenging, but is crucial in the perspective of future treatments. Clinical diagnostic criteria are currently based on the clinical examination and neuropsychological assessment, with the identification of dementia and then of the Alzheimer's phenotype (Blenow et al., 2006). Patients suffering from AD at a prodromal stage are, mostly, clinically classified as amnestic mild cognitive impairment (MCI) (Petersen et al., 1999; Dubois and Albert, 2004), but not all patients with amnestic MCI will develop AD. Recently, more precise research criteria were proposed for the early diagnostic of AD at the prodromal stage of the disease (Dubois et al., 2007). These criteria are based on a clinical core of early episodic memory impairment and the presence of at least one additional supportive feature including abnormal MRI and PET neuroimaging or abnormal cerebrospinal fluid amyloid and tau biomarkers (Dubois et al., 2007). Neuroimaging therefore adds a positive predictive value to the diagnosis and includes measurements using structural MRI to assess medial temporal lobe atrophy and positron emission tomography using fluorodeoxyglucose (FDG) or amyloid markers (Fox et al., 2004; Jagust, 2006)

Many groups studies based on volumetric measurements of regions of interest (ROI) (Convit et al., 1997, 2000; Jack et al., 1997,1998; Juottonen et al., 1998; Laakso et al., 1998, 2000; Busatto et al., 2003; Xu et al., 2000; Good et al., 2002; Chételat and Baron, 2003; Rusinek et al., 2004; Tapiola et al., 2008), voxel-based morphometry (Good et al., 2002; Busatto et al., 2003; Karas et al., 2003, 2004; Chételat et al., 2005; Whitwell et al., 2007, 2008) or group comparison of cortical thickness (Thompson et al., 2001, 2003, 2004; Lerch et al., 2005, 2008; Bakkour et al., 2009, Dickerson et al., 2009; Hua et al., 2009; McDonald et al., 2009) have shown that brain atrophy in AD and prodromal AD is spatially distributed over many brain regions including the entorhinal cortex, the hippocampus, lateral and inferior temporal structures, anterior and posterior cingulate.

However these analyses measure group differences and thus are of limited value for individual diagnosis.

Advances in statistical learning with the development of new machine learning algorithms capable of dealing with high dimensional data, such as the support vector machine (SVM) (Vapnik, 1995; Shawe-Taylor and Cristianini, 2000; Schölkopf and Smola, 2001), enables the development of new diagnostic tools based on T1-weighted MRI. Recently, several approaches have been proposed to automatically classify patients with AD and/or MCI from anatomical MRI (Fan et al., 2005, 2007, 2008a, 2008b; Colliot et al., 2008; Davatzikos et al., 2008a, 2008b; Klöppel et al., 2008; Vemuri et al., 2008; Chupin et al., 2009a, 2009b; Desikan et al., 2009; Gerardin et al., 2009; Hinrichs et al., 2009; Magnin et al., 2009; Misra et al., 2009; Querbes et al., 2009). These approaches could have the potential to assist in the early diagnosis of AD. These approaches can roughly be grouped into three different categories, depending on the type of features extracted from the MRI (voxel-based, vertex-based or ROI-based). In the first category, the features are defined at the level of the MRI voxel. Specifically, the features are the probability of the different tissue classes (grey matter, white matter and cerebrospinal fluid) in a given voxel (Lao et al., 2004; Fan et al., 2007, 2008a, 2008b; Davatzikos et al., 2008a, 2008b; Klöppel et al., 2008; Vemuri et al., 2008; Hinrichs et al., 2009; Magnin et al., 2009; Misra et al., 2009). Klöppel et al. (2008) directly classified these features with an SVM. All other methods first reduce the dimensionality of the feature space relying on different types of features extraction, agglomeration and/or selection methods. Vemuri et al. (2008) used smoothing, voxel-downsampling, and then a feature selection step. Another solution is to group voxels into anatomical regions through the registration of a labeled atlas (Lao et al., 2004; Ye et al., 2008; Magnin et al., 2009). However, this anatomical parcellation may not be adapted to the pathology. In order to overcome this limitation, Fan et al. (2007) have proposed an adaptive parcellation approach in which the image space is divided into the most discriminative regions. This method has been used in several studies (Davatzikos et al., 2008a, 2008b; Fan et al., 2008a, 2008b; Misra et al., 2009). In the second category, the features are

defined at the vertex-level on the cortical surface (Desikan et al., 2009; Querbes et al., 2009). The methods of the third category include only the hippocampus. Their approach is based on the analysis of the volume and/or shape of the hippocampus (Colliot et al., 2008, Chupin et al., 2009a, 2009b; Gerardin et al., 2009).

These approaches achieve high accuracy (over 84%). However, they were evaluated on different study populations, making it difficult to compare their respective discriminative power. Indeed, many factors such as degree of impairment, age, gender, genotype, educational level and MR image quality perceptibly affect the evaluation of the prediction accuracy. This variability between evaluations is increased for statistical reasons when the number of subjects is small. Therefore a meta-analysis would be of limited value to compare the prediction accuracies of different methods.

The goal of this paper was to compare different methods for the classification of patients with AD based on anatomical MRI, using the same study population. To that purpose, we used the Alzheimer's Disease Neuroimaging Initiative (ADNI) database. Ten methods were evaluated. We tested five voxel-based approaches: a direct approach (Klöppel et al., 2008), an approach based on a volume of interest (Klöppel et al., 2008), an atlas-based approach (Magnin et al, 2009) and the approaches proposed by Vemuri et al. (2008) and Fan et al. (2008a, 2008b) respectively. In order to assess the influence of the registration step and the features used on the classification accuracies, these latter methods were tested with two different registration steps: SPM5 (Ashburner and Friston, 2005) and DARTEL (Ashburner, 2007) and also with either only the grey matter (GM) probability maps or all the tissues probability maps including also white matter (WM) and cerebrospinal fluid (CSF). Three cortical approaches were evaluated as well: a direct one similar to (Klöppel et al., 2008), an atlas based one and an approach using only the regions found in (Desikan et al., 2009). Two methods respectively based on the volume (Colliot et al., 2008, Chupin et al., 2009a, 2009b) and the shape (Gerardin et al., 2009) of the hippocampus were also tested.

Materials

Data

Data used in the preparation of this article were obtained from the Alzheimer's disease Neuroimaging Initiative (ADNI) database (www.loni.ucla.edu/ADNI). The ADNI was launched in 2003 by the National Institute on Aging (NIA), the National Institute of Biomedical Imaging and Bioengineering (NIBIB), the Food and Drug Administration (FDA), private pharmaceutical companies and non-profit organizations, as a $60 million, 5-year public-private partnership. The primary goal of ADNI has been to test whether serial magnetic resonance imaging (MRI), positron emission tomography (PET), other biological markers, and clinical and neuropsychological assessment can be combined to measure the progression of mild cognitive impairment (MCI) and early Alzheimer's disease (AD). Determination of sensitive and specific markers of very early AD progression is intended to aid researchers and clinicians to develop new treatments and monitor their effectiveness, as well as lessen the time and cost of clinical trials.

MRI acquisition

The MR scans are T1-weighted MR images. MRI acquisition had been done according to the ADNI acquisition protocol in (Jack et al., 2008). For each subject, we used the MRI scan from the baseline visit when available and from the screening visit otherwise. We only used images acquired at 1.5 T. To enhance standardization across sites and platforms of images acquired in the ADNI study, pre-processed images that have undergone some post-acquisition correction of certain image artifacts are available (Jack et al., 2008). We used those corrected in image geometry for gradient nonlinearity and corrected for intensity non-uniformity due to non-uniform receiver coil sensitivity. The image geometry correction was the 3D gradwarp correction (Hajnal et al., 2001; Jovicich et al. 2006). The B1 non-uniformity correction is detailed in (Narayana et al., 1988). These two preprocessing steps can be performed directly on the MRI console and thus seem feasible in clinical routine. All subjects were scanned twice at each visit. As explained in (Jack et al., 2008), MR scans

were graded qualitatively by the ADNI investigators of the ADNI MRI quality control center at the Mayo Clinic for artifacts and general image quality. Each scan was graded on several separate criteria: blurring/ghosting, flow artifact, intensity and homogeneity, signal-to-noise ratio (SNR), susceptibility artifacts, and gray-white/cerebrospinal fluid contrast. For each subject, we used the MRI scan which was considered as the "best" quality scan by the ADNI investigators. In the description of the ADNI methods (http://www.loni.ucla.edu/ADNI/Data/ADNI_Data.shtml), the "best" quality image is the one which was used for the complete pre-processing steps. We thus used the images which had been selected for the complete pre-processing pipeline. No other exclusion criteria based on image quality were applied. The identification numbers of the images used in this study are reported in Tables S2 to S9.

Participants

The criteria used for the inclusion of participants were those defined in the ADNI protocol (described in details at http://www.adni-info.org/Scientists/AboutADNI.aspx#). Enrolled subjects were between 55-90 (inclusive) years of age, had a study partner able to provide an independent evaluation of functioning, and spoke either English or Spanish. All subjects were willing and able to undergo all test procedures including neuroimaging and agreed to longitudinal follow up. Specific psychoactive medications were excluded. General inclusion/exclusion criteria were as follows: Control subjects (CN) had MMSE scores between 24 and 30 (inclusive), a CDR (Clinical Dementia Rating) (Morris, 1993) of zero. They were non-depressed, non MCI, and non-demented. MCI subjects had MMSE scores between 24 and 30 (inclusive), a memory complaint, had objective memory loss measured by education adjusted scores on Wechsler Memory Scale Logical Memory II (Wechsler, 1987), a CDR of 0.5, absence of significant levels of impairment in other cognitive domains, essentially preserved activities of daily living, and an absence of dementia. AD patients had MMSE scores between 20 and 26 (inclusive), CDR of 0.5 or 1.0, and met NINCDS/ADRDA criteria for probable AD (McKhann et al., 1984).

We selected all the subjects for whom preprocessed images were available. The identification numbers of the subjects used in this study are reported in Tables S2 to S9. As a result, 509 subjects were selected: 162 cognitively normal elderly controls (CN) (76 males, 86 females, age ± SD = 76.3 ± 5.4 years, range = 60–90 years, mini-mental score (MMS) = 29.2 ± 1.0, range = 25–30), 137 patients with AD (67 males, 70 females, age ± SD = 76.0 ± 7.3 years, range = 55–91 years, MMS = 23.2 ± 2.0, range = 18–27), 76 patients with MCI who had converted to AD within 18 months (MCIc) (43 males, 33 females, age ± SD = 74.8 ± 7.4 years, range = 55–88 years, MMS = 26.5 ± 1.9, range = 23–30) and 134 patients with MCI who had not converted to AD within 18 months (MCInc) (84 males, 50 females, age ± SD = 74.5 ± 7.2 years, range = 58–88 years, MMS = 27.2 ± 1.7, range = 24–30). We did not consider MCI patients who had been followed less than 18 months and had not converted within this time frame. The 509 images came from 41 different centers.

To assess differences in demographic and clinical characteristics between groups, we used Student's t-test for age and MMS and Pearson's chi-square test for gender. Significance level was set at 0.05. No significant differences were found except for the MMS between controls and patients (AD or MCIc, $p<0.0001$).

In order to obtain unbiased estimates of the performances, the set of participants was then randomly split up into two groups of the same size: a training set and a testing set. The algorithms were trained on a training set and the measures of the diagnostic sensitivity and specificity were carried out with an independent test set. The division process preserved the age and sex distribution.

Demographic characteristics of the studied population selected from the ADNI database are presented in Table 1.

Methods

Classification experiments

Three classification experiments were performed to compare the different approaches. The first one is the classification between CN subjects and patients with probable AD and is referred to as "CN *vs* AD" in the following. The second one is the classification between CN subjects and MCI converters and is referred to as "CN *vs* MCIc". It corresponds to the detection of patients with prodromal AD as defined by (Dubois and Albert, 2004). Indeed, MCI patients who will convert to AD are, at baseline, patients with incipient AD but non-demented, i.e. patients with prodromal AD. The third one is the classification MCInc versus MCIc and is referred to as "MCInc *vs* MCIc". It corresponds to the prediction of conversion in MCI patients.

Classification methods

The different approaches we compared can be grouped into three categories with respect to the features used for the classification. In the first category, the features are defined at the level of the MRI voxel. Specifically, the features are the probability of the different tissue classes (GM, WM and CSF) in a given voxel. In the second category, the features are defined at the vertex-level on the cortical surface. Specifically, the features are the cortical thickness at each vertex of the cortex. The methods of the third category include only the hippocampus.

These methods are summarized in Table 2 and briefly presented in the following paragraphs.

First category: voxel-based segmented tissue probability maps

The features of the methods of the first category were computed as follows. All T1-weighted MR images were spatially normalized and segmented into GM, WM and CSF using the SPM5 (Statistical Parametric Mapping, London, UK) unified segmentation routine (Ashburner and Friston, 2005) with the default parameters. These maps constitute a first set of tissue probability maps and will be referred to respectively as SPM5_GM, SPM5_WM and SPM5_CSF.

To evaluate the impact of the registration step on the classification accuracy, the GM and WM probability maps in native space segmented by the SPM5 unified segmentation routine were also normalized to the population template generated from all the images, using the DARTEL diffeomorphic registration algorithm (Ashburner, 2007) with the default parameters. The obtained transformations were applied to the GM, WM and CSF tissue maps. These maps compose a second set of tissue probability maps and will be referred to respectively as DARTEL_GM, DARTEL_WM and DARTEL_CSF. Some papers used only GM maps while others included all three tissues. In our experiments, we systematically evaluated the added value of WM and CSF maps by comparing the classification obtained with only GM to that obtained with all three classes. All maps were then modulated to ensure that the overall tissue amount remains constant. No spatial smoothing was performed, unless when otherwise specified.

The different methods of this category differ by the way the features are extracted and/or selected from the voxel probability maps. This is detailed in the following paragraphs.

Direct

The simplest approach consists in considering the voxels of the tissue probability maps directly as features in the classification. This type of approach is referred to as "*Voxel-Direct*" in the following. Such an approach was proposed by Klöppel et al. (2008) with two different versions: one is based on whole brain datasets and the other includes only data from a volume of interest (VOI) located in the anterior medial temporal lobe, including part of the hippocampus. This volume of interest was defined as two rectangular cuboids centered on x = -17, y = -8, z = -18 and x = 16, y = -9, z = -18 in the MNI space. Their dimensions were 12 mm, 16 mm and 12 mm in the x, y and z directions respectively. The latter method will be referred to as "*Voxel-Direct_VOI*". In their paper, they used only DARTEL_GM maps. Here, we will test all approaches with the following sets of probability maps: SPM5_GM only, SPM5_GM and SPM5_WM and SPM5_CSF, DARTEL_GM only, DARTEL_GM, and DARTEL_WM and DARTEL_CSF.

STAND-score

Vemuri et al. (2008) proposed an approach called the STAND score, in which the dimensionality is reduced by a sequence of feature aggregation and selection steps. First, the tissue probability maps were smoothed and down-sampled by averaging. Then, voxels that contained less than 10% tissue density values and CSF in half or more of the images were not considered for further analysis. A feature selection step was then carried out. First, a linear SVM was applied for each tissue class, which attributes a weight to each feature. Only features of which weights are consistent with increased neurodegeneration in the pathological group were kept. Then a second feature selection step was performed on the remaining features. To ensure spatial consistency, neighboring voxels of the voxels selected so far were also selected. The features from the different tissue classes were concatenated and then used in the classification. This approach is referred to as "*Voxel-STAND*" in the following. In their paper, the features used for this approach were the GM, WM and CSF tissue probability maps segmented and registered with the SPM5 unified segmentation routine using a customized tissue probability maps. Thus we also tested the classification with customized tissue probability maps.

Atlas based

Another approach consists in grouping the voxels into anatomical regions using a labeled atlas. This type of approach is used in (Lao et al., 2004; Magnin et al., 2009). Each tissue probability map in the stereotaxic space was parceled into 116 regions of interest (ROI) using the AAL (Automatic Anatomical Labeling) atlas (Tzourio-Mazoyer et al., 2002). In each ROI, we computed the mean tissue probability and used these values as features in the classification. Such an approach will be referred to as "*Voxel-Atlas*". Note that the AAL is a predefined anatomical atlas, which has not been specifically designed for studying patients with AD; its areas thus do not necessarily represent pathologically homogeneous regions.

COMPARE

Instead of using a predefined atlas, Fan et al. (2007, 2008a, 2008b) proposed a parcellation that is adapted to the pathology. The thorough explanation of the method is in (Fan et al., 2007). Very briefly, the concept of COMPARE is to create homogeneously discriminative regions. In these regions, the voxel values are aggregated to form the features of the classification. Feature selection steps are then performed to identify the most discriminative regions. In the following, we refer to this approach as "*Voxel-COMPARE*". We used the COMPARE software freely available on request for download online (https://www.rad.upenn.edu/sbia/software/index.html).

Second category: cortical thickness

In this second category, the features are the cortical thickness values at each vertex of the cortical surface. Cortical thickness represents a direct index of atrophy and thus is a potentially powerful candidate to assist in the diagnosis of AD (Thompson et al., 2001, 2003, 2004; Lerch et al., 2005, 2008; Bakkour et al., 2009; Dickerson et al., 2009; Hua et al., 2009; McDonald et al., 2009). Cortical thickness measures were performed with the FreeSurfer image analysis suite (Massachusetts General Hospital, Boston, MA), which is documented and freely available for download online (http://surfer.nmr.mgh.harvard.edu/). The technical details of this procedure are described in (Sled et al., 1998; Dale et al., 1999; Fischl et al., 1999a, 1999b; Fischl and Dale, 2000). All the cortical thickness maps were registered onto the default FreeSurfer common template. Four subjects were not successfully processed by the FreeSurfer pipeline. Those subjects are marked by an asterisk in Tables S2 to S9. They could thus not be classified with the SVM and were excluded from the training set. For the testing set, the subjects were considered as 50% misclassified.

Direct

As in (Klöppel et al., 2008) for voxel-based maps, the simplest way consists in considering cortical

105 thickness values at every vertices directly as features in the classification with no other
106 preprocessing step. This approach is referred to as "*Thickness-Direct*" in the following.
107
108 *Atlas based*
109 As in the voxel-based case, we also tested an approach where vertices are grouped into anatomical
110 regions using an atlas. Such approach is used in (Querbes et al., 2009, Desikan et al., 2009). The
111 cortical parcellation was carried out with the cortical atlas of (Desikan et al., 2006). The atlas is
112 composed of 68 gyral based ROIs. In each ROI, we computed the mean cortical thickness and used
113 these values as features in the classification. This approach is referred to as "*Thickness-Atlas*" in the
114 following.
115
116 *ROI*
117 Desikan et al. (2009) parcellated the brain into neocortical and non-neocortical ROIs by wrapping
118 an anatomical atlas (Desikan et al., 2006). They studied the discriminative power for CN versus
119 MCIc of the mean thickness (neocortical regions) and the volume (both neocortical and non-
120 neocortical regions). For their analysis, the mean thickness and the volumes of the right and the left
121 hemispheres, for each ROI, were added together. The volumes were corrected using estimate of the
122 total intracranial volume.
123 Their study was carried out on a cohort of 97 participants selected from the Open Access Series of
124 Imaging Studies (OASIS) database (Marcus et al., 2007). They found out that, with a logistic
125 regression analysis, the best set of discriminator was: the entorhinal cortex thickness, the
126 supramarginal gyrus thickness and the hippocampal volume. They used these features with a
127 logistic regression to classify CN and MCIc and to classify CN and AD. Therefore, in this approach,
128 we used only these three features for the classification. This approach is referred to as "*Thickness-*
129 *ROI*" in the following.
130

Third category: hippocampus

Finally, we tested the discriminative power of methods which consider only the hippocampus and not the whole brain or the whole cortex as in the two first categories. The hippocampus is affected at the earliest stages of the disease and has thus been used as a marker of early AD in a vast number of studies.

Here, the segmentation of the hippocampus was performed using SACHA, a fully automatic method we previously developed (Chupin et al., 2007, 2009a). This approach has been shown to be competitive with manual tracing for the discrimination of patients with AD and MCI (Colliot et al., 2008; Chupin et al., 2009b). This approach segments both the hippocampus and the amygdala simultaneously based on competitive region-growing between these two structures. It includes prior knowledge on the location of the hippocampus and the amygdala derived from a probabilistic atlas and on the relative positions of these structures with respect to anatomical landmarks which are automatically identified.

We also evaluated the hippocampal volume obtained with the FreeSurfer image analysis suite.

Volume

We first tested the classification accuracy obtained when the only feature is the hippocampal volume. For each subject, we computed the volume of the hippocampi. Volumes were normalized by the total intracranial volume (TIV) computed by summing SPM5 segmentation maps of grey matter, white matter, and cerebrospinal fluid (CSF), inside a bounding box defined in standard space to obtain a systematic inferior limit. For more robustness with respect to segmentation errors, left and right volumes were averaged. The thorough explanation of the method is in (Chupin et al., 2007, 2009a, 2009b). This approach is referred to as "*Hippo-Volume-S*" in the following.

We also evaluated this approach with the hippocampal volume obtained with the FreeSurfer image analysis suite and corrected with the total intracranial volume also obtained with obtained with FreeSurfer. This approach will be referred to as "*Hippo-Volume-F"*.

Shape

We then tested an approach in which the features describe the hippocampal shape (Gerardin et al., 2009). Each hippocampus was described by a series of spherical harmonics (SPHARM) to model the shape of the segmented hippocampi. The classification features were based on the SPHARM coefficients. Specifically, each subject was represented by two sets (one for each hippocampus) of three-dimensional SPHARM coefficients. The SPHARM coefficients were computed using the SPHARM-PDM (Spherical Harmonics-Point Distribution Model) software developed by the University of North Carolina and the National Alliance for Medical Imaging Computing (http://www.namic.org/Wiki/index.php/Algorithm:UNC:Shape_Analysis). In the original paper by our group describing this method (Gerardin et al., 2009), we used a feature selection step because the subjects groups were much smaller (less than 30 subjects in each group). When the number of subjects is small, the classifier can be more sensitive to uninformative features. In the present study, the number of subjects was larger and thus a feature selection step is less necessary and increases the risk of overfitting. We thus chose to avoid this selection step. We also tested the procedure with the selection step but it did not lead to further improvement in this study. Moreover, the degree of the SPHARM decomposition was set at four. Four subjects were not successfully processed by the SPHARM pipeline. Those subjects are marked by a dagger in Tables S2 to S9. They could thus not be classified with the SVM and were excluded from the training set. For the testing set, those subjects were considered as 50% misclassified. This approach is referred to as "*Hippo-Shape*" in the following.

Classification using SVM

Classifiers

A support vector machine is a supervised learning method. In brief: given a training set of size K: $(x_k, y_k)_{k=1...K}$, where x_k in $\boldsymbol{R}^d$ are observations, and y_k in $\{-1,1\}$ are corresponding labels, SVMs search for the optimal margin hyperplane (OMH) separating groups, i.e. the hyperplane for which the margin between groups is maximal. More details on SVM can be found in (Vapnik 1995; Shawe-Taylor and Cristianini, 2000, 2004; Schölkopf and Smola, 2001). We used a linear C-SVM for all the approaches except COMPARE (Fan et al., 2007) for which a non-linear C-SVM with a Gaussian kernel was used. The SVM implementation relied on the LIBSVM Library (Chang and Lin, 2001).

The dimension of the features of the approach *Hippo-Volume* is only one. Therefore a much simpler classifier can be used with no hyperparameter: each participant is assigned to the closest group. Specifically, if S_1 and S_2 are two groups of participants with respective centers of mass defined as m_1 and m_2, a new individual with hippocampus volume x is assigned to the closest group according to its Euclidean distance to the center of mass. This is a Parzen window classifier with the linear kernel and assuming a prevalence of 50% (Shawe-Taylor and Cristianini, 2004).

As in (Desikan et al., 2009) a logistic regression is used instead of a SVM, the classification step of *Thickness-ROI* was also based on a logistic regression.

Evaluation

In order to obtain unbiased estimates of the performances, the set of participants was randomly split into two groups of the same size: a training set and a testing set. The division process preserves the age and sex distribution. The training set was used to determine the optimal values of the hyperparameters of each method and to train the classifier. The testing set was then only used to evaluate the classification performances. The training and testing sets were identical for all

methods, except for those four cases for which the cortical thickness pipeline failed and those other four for which the SPHARM pipeline failed. For the SPHARM and the cortical thickness methods, the subjects for whom the corresponding pipeline failed could not be classified with the SVM and were therefore excluded from the training set. As for the testing set, since those subjects were neither misclassified nor correctly classified, they were considered as 50% misclassified. This approach was chosen because a failure of the pipeline is a weakness of the methods.

On the training set, cross-validation (CV) was used to estimate the optimal values of hyperparameters. In general, there is only one hyperparameter which is the cost parameter C of the linear C-SVM. In *Voxel-STAND*, there is a second parameter which is the threshold t of feature selection. In *Voxel-COMPARE*, a second parameter is the size σ of the Gaussian kernel and the third parameter is the number n of selected features. In *Hippo-Volume*, there is no hyperparameter. The optimal parameters values were determined using a grid-search and leave-one-out cross validation (LOOCV) on the training set. The grid search was performed over the ranges $C = 10^{-5}, 10^{-4.5}, ..., 10^{2.5}, 10^{3}$, $t = 0.06, 0.08, ..., 0.98$, $\sigma = 100, 200, ..., 1000$ and $n = 1, 2, ..., 150$ (except for *Voxel-COMPARE* were $C=10^{0}, 10^{1}, 10^{1.5}, 10^{2}, 10^{2.5}$).

For each approach, the optimized set of hyperparameters was then used to train the classifier using the training group; the performance of the resulting classifier was then evaluated on the testing set. In this way, we achieved unbiased estimates of the performances of each method.

For each method, we computed the number of true positives TP (i.e. the number of diseased individuals which were correctly identified by the classifier), the number of true negatives TN (i.e. the number of healthy individuals which were correctly identified by the classifier), the number of false positives FP (i.e. the number of healthy individuals which were not correctly identified by the classifier), the number of false negatives FN (i.e. the number of diseased individuals which were not correctly identified by the classifier). We then computed the sensitivity defined as TP/(TP+FN), the specificity defined as TN/(TN+FP), the positive predictive value defined as PPV=TP/(TP+FP), the negative predictive value defined as NPV=TN/(TN+FN). Finally it should be noted that the

number of subjects in each group is not the same. The classification accuracy does not enable to compare the performances between the different classification experiments. Thus we considered both the specificity and the sensitivity instead.

To assess whether each method performs significantly better than a random classifier, we used McNemar's chi square tests. Significance level was set at 0.05. We also used McNemar's chi square tests to assess differences between DARTEL and SPM5 registrations and between classification results obtained using only GM and using all three maps. The McNemar test investigates the difference between proportions in paired observations. We used it to assess the difference between proportions of correctly classified subjects, i.e. accuracy. The corresponding contingency table is presented in Table 3.

Results

Classification results

The results of the classification experiments are summarized in Tables 4, 5 and 6 respectively for CN *vs* AD, CN *vs* MCIc and CN *vs* MCInc. The classification results of CN *vs* AD and CN *vs* MCIc are also represented in Figure 1. In each table, the different methods are referred to either by their abbreviation or by their number defined in Table 2.

CN vs AD

The classification results for CN *vs* AD are summarized in Table 4 and in Figure 1. All methods performed significantly better than chance ($p<0.05$). The four *Voxel* methods (Voxel-Direct, *Voxel-STAND*, *Voxel-Atlas*, *Voxel-COMPARE*) classified AD from CN with very high specificity (over 89%) and high sensitivity: 75% for *Voxel*-STAND and over 81% for the other three methods. Methods based on the cortical thickness led to similar results with at least 90% specificity and 69%, 74% and 79% respectively for *Thickness-ROI*, *Thickness-Direct* and *Thickness-Atlas*. The hippocampus-based strategies were as sensitive but less specific: between 63% for *Hippo-Volume* and 84% for *Hippo-Shape.*

CN vs MCIc

Classification results for CN *vs* MCIc are summarized in Table 5 and in Figure 1. Most methods were substantially less sensitive than for AD vs CN classification. All methods except *Voxel-COMPARE* and the *Hippo* methods obtained significantly better results than a random classifier ($p<0.05$). There was no substantial difference between the results obtained with *Voxel-Direct*, *Voxel-Atlas* and *Voxel-STAND*. All those methods reached a high specificity (over 85%) but a sensitivity ranging between 51% (*Voxel-COMPARE*) and 73% (*Voxel-STAND*). The methods based on cortical thickness behave as well as the previous ones. *Hippo-Volume* was slightly less specific but as sensitive as for the AD *vs* CN classification.

MCInc vs MCIc

The classification results for MCInc *vs* MCIc are summarized in Table 5. Only four methods managed to predict conversion slightly more accurately than a random classifier but none of them got significantly better results ($p>0.05$). *Thickness-Direct* reached 32% sensitivity and 91% specificity. *Voxel-STAND* reached 57% sensitivity and 78% specificity, *Voxel-COMPARE* reached 62% sensitivity and 67% specificity. *Hippo-Volume* distinguished MCIc from MCInc with 62% sensitivity and 69% specificity.

Influence of the preprocessing

To evaluate the impact of the registration step, we tested both the registration using SPM5 unified segmentation and the registration DARTEL as described in the previous section. The influence of the registration step on the classification results is illustrated on Figures 2 and 3. The performances obtained for the MCInc *vs* MCIc experiment were too low to be used to evaluate the impact of the registration step. Therefore we did not take them into account for this comparison. The use of the diffeomorphic registration algorithm DARTEL significantly improved the results of six out of 20 classification experiments ($p<0.05$). On the other hand, it led to significantly worse results in two cases. According to the results in Tables 4, 5, 6, the use of customized tissue probability maps for the registration with SPM5 unified segmentation did not improve the results of *Voxel-STAND*.

We also compared the classification obtained with only the GM maps to those with GM, WM and CSF maps. Results are presented on Figures 2 and 3. The use of all three maps led to significantly worse results ($p<0.05$) for two out of 20 classification experiments (*Voxel-Direct_VOI-S* and *Voxel-COMPARE-D*). It never led to significantly better results.

Complementariness of the methods

The different approaches tested tackle the classification problem with various angles and could thus be complementary. In order to quantify their similarity, we used the Jaccard similarity coefficient

(Jaccard, 1901; Shattuck et al., 2001). In this case, the Jaccard index of two methods is the number of subjects correctly classified by both methods divided by the number of subjects correctly classified by at least one of the two methods. Results are presented on Figures S1 and S2. All methods are in at least substantial agreement (Jaccard over 0.6) and most of them are in strong agreement. The most different results were obtained with the methods relying on the hippocampus.

We tested the combination of three approaches, one of each strategy: *Voxel-Direct-D-gm*, *Thickness-Atlas* and *Hippo-Volume-S*. A convenient approach to combine different SVM-based methods is to consider that the resulting classifier is a SVM which kernel is a linear convex combination of the kernels of each method. The problem of learning both the coefficients of the best convex linear combination of kernels and the optimal margin hyperplane (OMH) is known as the multiple kernel learning (MKL) problem (Lanckriet et al., 2004; Bach et al., 2004; Sonnenburg et al., 2006). We used the SimpleMKL toolbox (Rakotomamonjy et al., 2008). All four possible combinations have been tested. The kernels are normalized with the trace of the Gram matrix of the training set. Note that for *Hippo-Volume-S*, the Parzen window classifier is replaced by a linear SVM.

None of these four combinations improved the accuracy in the CN *vs* AD experiment. Only the combination of *Hippo-Volume-S* and *Thickness-Atlas* improved only slightly the accuracy for the CN *vs* MCIc and the MCInc *vs* MCIc experiments. It distinguished MCIc from CN with 76% sensitivity and 85% specificity. The optimal coefficients of the linear combination were 0.057 and 0.943 for the kernels of *Hippo-Volume-S* and *Thickness-Atlas,* respectively. This combination classified MCIc and MCInc with 43% sensitivity and 83% specificity. The optimal coefficients of the linear combination were 0.030 and 0.970 respectively.

Influence of age and gender on classification results

We investigated whether the age of the subjects influences the classification results. We thus computed the average age of true positives, false positives, true negatives and false negatives.

Overall, we found that the false positives were often older than the true negatives, meaning that the oldest controls were more often misclassified. Specifically, this was the case for 25 methods over 28 for CN *vs* AD and 24/28 for CN *vs* MCIc. Conversely, false negatives were often younger than the true positives, meaning that the youngest patients were more often misclassified. Specifically, this was the case for 26 methods over 28 for CN *vs* AD and 28/28 for CN *vs* MCIc. The number of misclassified subjects was too small to test for statistical significance of these differences. However, the fact that this difference was present for the vast majority of method suggests that it may not be due to chance. We also investigated the influence of gender but did not find any difference.

Computation time

The computations were carried out with a processor running at 3.6 GHz with 2GB of RAM. Table 7 presents, for each method, the order of magnitude of the computation time (i.e. minutes, hours, days, weeks). For each method, we report the computation time of its three main phases: the feature computation step (segmentation, registration), the building of the classifier (including the grid search for the optimization of the hyperparameters and the learning of the classifier), and the classification of a new subject.

The order of magnitude of the computation time for the tissue segmentation and the registration step per subject is respectively about ten minutes and an hour with SPM5 and DARTEL. The cortical thickness computation and the registration of a single subject with FreeSurfer take roughly a day. The segmentation of the hippocampi of a subject lasts a few minutes and the shape analysis process with the SPHARM decomposition about one hour. The tuning of parameters and learning phase took from a few minutes to several weeks for the *Voxel-STAND* and *Voxel-COMPARE* methods. Once the hyperparameters are set and the learning is done, it takes at most minutes to classify a new subject.

Optimal margin hyperplanes

105 The classification function obtained with a linear SVM is the sign of the inner product of the
106 features with w, a vector orthogonal to the optimal margin hyperplane (OMH) (Vapnik 1995;
107 Shawe-Taylor and Cristianini, 2000, 2004; Schölkopf and Smola, 2001). Therefore if the i^{th}
108 component w_i of the vector w is small, the i^{th} feature will have a small influence on the
109 classification. Conversely, if w_i is large, the i^{th} feature will play an important role in the classifier.
110 When the input features are the voxels of the image, each component of w also corresponds to a
111 voxel. One can thus represent the values of w in the image space. Similarly, for the *Thickness*
112 methods, the values of w can be represented on the cortical surface. The values of the optimal
113 margin hyperplanes for the different methods are presented on Figures from 4 to 7. This allows a
114 qualitative comparison of the features used in the classifier. Our aim was not to perform a statistical
115 analysis of differences between groups - for example using permutation tests on the coefficients
116 (Mourão-Miranda et al., 2005).

117 Figures 4 and 5 show the OMH for CN *vs* AD and CN *vs* MCIc respectively for the *Voxel*
118 methods. Overall, the spatial patterns corresponding to CN *vs* AD and CN *vs* MCIc are similar. For
119 *Voxel-Direct-D-gm*, the main regions were the medial temporal lobe (hippocampus, amygdala and
120 the parahippocampal gyrus), the inferior and middle temporal gyri, the posterior cingulate gyrus and
121 the posterior middle frontal gyrus. To a lesser extent, the OMH also included the inferior parietal
122 lobule, the supramarginal gyrus, fusiform gyrus, the middle cingulate gyrus and in the thalamus.
123 When all three tissue maps were used, the CSF maps mirrored the GM map (the enlargement of the
124 ventricle mirroring GM reduction). This was also the case for part of the WM map, in particular in
125 the hippocampal region. When using SPM5 unified segmentation instead of DARTEL, voxels were
126 much more scattered and not grouped into anatomical regions except in the medial temporal lobe.
127 For the AAL atlas, regions included the hippocampus, the amygdala, the parahippocampal gyrus,
128 the cingulum, the middle and inferior temporal gyri and the superior and inferior frontal gyri. The
129 regions were very similar for the surface Atlas as shown on Figure 6. Regions corresponding to
130 *Thickness-Direct* (Figure 7) were more restricted: the entorhinal cortex, the parahippocampal gyrus

and to a lesser extent the lateral temporal lobe, the inferior parietal lobule and some prefrontal areas.

Optimal parameters of the classifiers

For each approach, the optimal values of the hyperparameters are summarized in Table S1. One should note that the *Hippo-Volume* method has no hyperparameter.

Discussion

In this paper, we compared different methods for the classification of patients with AD and MCI based on anatomical T1-weighted MRI. To evaluate and compare the performances of each method, three classification experiments were performed: CN *vs* AD, CN *vs* MCIc and CN *vs* MCInc. The set of participants was randomly split up into two groups of the same size: a training set and a testing set. For each approach, the optimal parameter values had been determined using a grid-search and LOOCV on the training set. Those values were then used to train the classifier using the training group; the performance of the resulting classifier was then evaluated on the testing set. In this way, we obtained unbiased estimates of the performances of each method.

Classification methods discriminate AD from normal aging

All the classification methods that we tested in this paper achieved accuracies significantly better than chance for the discrimination of patients with AD from normal aging. All methods except *Voxel-COMPARE* and *Hippo* methods performed significantly better than chance for the discrimination of patients with prodromal AD (MCIc) from normal aging. For AD *vs* CN, most methods achieved high sensitivity and specificity. However, at the prodromal stage, their sensitivity was substantially lower.

The classification results we obtained for AD *vs* CN with *Atlas* and *COMPARE* methods are lower than those reported in the respective papers: 94% accuracy for the *COMPARE* method in (Fan et al., 2008a) and 92% sensitivity and 97% specificity for the *Atlas* in Magnin et al. (2009). These differences can be explained by several factors. First, in the original papers, the hyperparameters were optimized on the testing set. This may lead to overfitting the testing set and thus to overestimate the sensitivity and specificity. On the contrary, in our evaluation, the learning step as well as the optimization of the hyperparameters had been carried out on a training set and the evaluation of the performance on a completely separated testing set. Thus our evaluation was unbiased. Another explanation may stem from differences between studied populations (sample

size, stage of the disease). In particular, the ADNI population includes a large number of subjects with vascular lesions, which was not the case in Magnin et al. (2009). Finally, the image preprocessing step may also have an impact on the classification results. Davatzikos et al. (2008b) and Fan et al. (2008b) used the RAVENS maps (Goldszal et al., 1998), thus the registration and the segmentation step was different and might lead to different classification results. However, the aim of the present paper was to compare different classification strategies and it was thus necessary to use the same preprocessing for all methods. Since most of them relied on SPM, we chose to use this preprocessing for all methods. It is possible that using other registration approaches such as HAMMER would increase the classification performance but this is beyond the scope of this paper.

For the *Voxel-STAND* and *Voxel-Direct* methods, our results were similar to those reported in the original papers by Vemuri et al. in (2008) and Klöppel et al. (2008). This can probably be explained by the fact that Vemuri et al.'s (2008) evaluation procedure is also based on independent testing group and that Klöppel et al. (2008) did not mention any optimization of the hyperparameters. As for the *Thickness-ROI,* the results (69% sensitivity and 94% specificity) were lower than those obtained by Desikan et al. (2009) (100% specificity and sensitivity). A possible explanation is that in their study the classifier was trained on a different population (patients with CDR=0.5) selected from a different database (the OASIS database).

The results obtained with Hippo-Volume were similar to those that we previously reported for the ADNI database (Chupin et al., 2009b). The sensitivities and specificities were however lower than those found in our previous study on a different population (Colliot et al., 2008) (84% sensitivity and specificity for CN *vs* AD). This can be explained by several factors (Chupin et al., 2009b). First ADNI is a multi-site database whereas the data in the previous study came from a single scanner. Moreover the population included a large number of subjects with vascular lesions. The slight difference between the results obtained in (Chupin et al., 2009b) and the present results mostly comes from the difference in the accuracy estimation: two separate groups instead of a LOOCV procedure. As for the *Hippo-Shape* method the results were substantially lower than our

results reported in (Gerardin et al., 2009) (86% for CN *vs* AD). This may result from the relatively small number of subjects used in our previous study. Besides, the estimation was carried out with a LOOCV. Moreover, this can also be due to that fact that all subjects were considered without taking into consideration the quality control (Chupin et al., 2009b) of the hippocampus segmentation.

To our knowledge, the classification CN *vs* MCIc has only been addressed by Desikan et al. (2009). Davatzikos et al. (2008a) and Fan et al. (2008a, 2008b) have performed the classification CN vs MCI with no distinction between converters and non-converters. The MCI group did not include only prodromal AD, hence the classification experiment cannot be compared to CN *vs* MCIc. Desikan et al. (2009) classified CN and MCI who converted within two years after baseline with 91% accuracy. This is substantially higher than the results obtained in our paper with the same method *Thickness-ROI* (65% sensitivity and 94% specificity).

Prediction of conversion in MCI patients

No method was able to predict conversion better than chance. The three most accurate methods were: *Voxel-STAND* (57% sensitivity and 78% specificity), *Voxel-COMPARE* (62% sensitivity and 67% specificity) and *Hippo-Volume* (62% sensitivity and 69% specificity). These three methods restricted their search to a portion of the brain. In *Voxel-STAND* and *Voxel-COMPARE*, this was done using feature selection: the selected regions are mainly in the medial temporal structures. In Hippo-Volume, this was done by considering only the hippocampus.

Even for these three methods, the performances remained particularly low. The main reason is certainly that MCI non converters are a very heterogeneous group: some patients would convert shortly after the end of the follow-up and are thus in fact prodromal AD patients while others would remain stable for a long period of time. We thus advocate that classification methods should be focused on the detection of prodromal AD (i.e. MCI converters) which is a much better defined entity.

To our knowledge, the classification MCInc *vs* MCIc has only been addressed by Misra et

al. (2009) and Querbes et al. (2009). Misra et al. (2009) considered the conversion within 12 months and Querbes et al. (2009) within 24 months. They obtained substantially higher accuracy: respectively 81.5% and 76% accuracy. Misra et al. (2009) used the COMPARE (Fan et al., 2007) classification methods. The differences may result from the same reasons as explained in the previous paragraph: the use of separate training and testing sets and differing preprocessing steps. Querbes et al. (2009) used a feature selection step, which may explain the slightly higher accuracy.

Whole brain or hippocampus?

For CN *vs* AD, methods using the whole brain (or the whole cortex) reached substantially higher specificity (over 90%) than those based on the hippocampus (from 63% to 84%). For the detection of prodromal AD, hippocampal-based approaches remained competitive with whole-brain methods. It thus seems that considering the whole brain is advantageous mostly at the most advanced stages. Indeed, at these more advanced stages, the atrophy is much more widespread. Moreover, it should be noted that many subjects included in the ADNI have vascular lesions which may be, at least partially, captured by whole brain methods. For intermediate stages, an alternative would be to consider a set of selected regions instead of the whole brain or the hippocampus alone. For example, *Thickness-ROI* performs at least as well as whole brain approaches for the detection of prodromal AD. Even though they achieve lower accuracies, hippocampal-based methods may still be of interest to the clinician because they provide a direct and easily interpretable index to the clinician (the hippocampal volume) while the whole-brain approaches base their classification on a complex combination of different regions.

All methods presented substantial agreement (Jaccard index over 0.6). The most different results were obtained between hippocampal and whole brain methods. However, combining them through multiple kernel learning did not improve the classification results.

The registration step: is a fully deformable method advantageous?

The use of DARTEL significantly improved the classification results in six cases, while it led to lower results in only two cases. This is in line with other studies which reported that DARTEL led to higher overlap values (Klein et al., 2009; Yassa and Stark, 2009) and higher sensitivity for voxel-based morphometry (Bergouignan et al., 2009). In particular, the use of a fully deformable method was advantageous for the medial temporal lobe as shown in (Yassa and Stark, 2009; Bergouignan et al., 2009). Since the hippocampus is highly affected in AD, we expected that using a method which registers the hippocampus better, would result in higher classification accuracy.

Does adding WM and CSF maps increase the performance of the classifiers?

In their original description, some of the tested methods used the three tissue (GM, WM and CSF) maps (e.g. Vemuri et al., 2008, Fan et al., 2007, Magnin et al., 2009) while others used only the GM maps (e.g. Klöppel et al., 2008). In this paper, we systematically tested whether the compared methods performed better with the three maps or with only the GM maps. It should be noted that this does not aim at assessing the diagnostic value of WM or CSF in general but only to test if including all tissue maps is more effective for these particular classification approaches under study. On the whole, adding the WM and the CSF probability maps did not improve the classification performances. Adding WM and CSF maps increases the dimensionality of the feature space which can make the classifier unstable and lead to overfitting the data. This problem is well-known in machine learning as the curse of dimensionality. Besides, elder subjects are likely to have WM structural abnormalities caused by leucoaraiosis or other diseases. Therefore adding WM tissues may add noise in the features. Even if WM structural abnormalities alter (Levy-Cooperman et al., 2008) the tissue segmentation step, GM probability maps are more robust features than WM tissues probability maps.

Adding the WM and the CSF in the features may improve the results in two instances. The first one is when the method encloses a feature selection step. Methods including feature selection

steps are more able to keep only the added value and avoid considering the noise but, overall, the improvement is not substantial. Adding WM and CSF may also improve the results of methods grouping the voxels into ROIs via wrapping a labelled atlas. It may make up for the parcellation error due to the registration step but, again, the improvement is not substantial.

Is it worth performing feature selection?

The main objectives of the feature selection step are to keep only informative features and to reduce the dimensionality of the feature space. In our evaluation, two methods included a feature selection step: Voxel-STAND and Voxel-COMPARE. Overall, these methods did not perform substantially better than simpler ones. In particular, their results might be more sensitive to the training set. Indeed, feature selection can be regarded as a learning step. In such a case, the feature selection step increases the class of all possible classification functions, which could lead to overfitting the data. A more robust way to decrease the dimensionality of the features way would be to use more prior knowledge of the disease.

Besides features selection can be time consuming as it adds new hyperparameters and thus makes the gridsearch less tractable. Compared to *Voxel-Direct* and *Voxel-Atlas*, *Voxel-STAND* and *Voxel-COMPARE* are time consuming (up to weeks), mostly because of the number of hyperparameters to be tuned.

Nevertheless, feature selection proved useful in two specific cases. First, these methods proved less sensitive when increasing the dimensionality of the feature space by adding WM and CSF maps. They also tended to be more accurate for the MCIc *vs* MCInc experiment, where only a few brain regions are informative.

Does age influence the classification accuracy?

Overall, we found that the oldest controls and the youngest patients were more often misclassified. This may results from different causes. Normal aging is associated with atrophy of the grey and

white matter and increase of the CSF (Good et al., 2001; Salat et al., 2004). Moreover, aging is also associated with alterations in tissue intensity and contrast, which can disrupt the segmentation step and thus artificially increase the measured atrophy (Salat et al., 2009). Besides, elderly subjects are more likely to have structural abnormalities of the white matter, which can also impede the tissue segmentation step (Levy-Cooperman et al., 2008) and increase the measured atrophy. In addition, elderly subjects have a propensity to suffer from mixed dementia (Zekry et al., 2002).

Optimal margin hyperplanes

In a linear SVM, the OMH can be easily represented. The OMH provides information about the regions of the brain which were used by the classifier. It should be noted that this only provides qualitative information on the hyperplanes, and that no statistical analysis of the OMH coefficients was performed.

With *Voxel-Direct-D*, *Voxel-Atlas* and *Thickness-Atlas*, the regions in which atrophy increased the likelihood of being classified as AD or MCIc were largely consistent with the pattern of atrophy demonstrated in previous morphometric studies. These regions included the medial temporal lobe, the inferior and middle temporal gyri (Chételat and Baron, 2003; Good et al., 2002; Busatto et al., 2003; Rusinek et al., 2004; Tapiola et al., 2008), the posterior cingulate gyrus (Karas et al., 2004; Chételat et al., 2005; Laakso et al., 1998) and the posterior middle frontal gyrus (Whitwell et al., 2007), the fusiform gyrus, the thalamus (Karas et al., 2003, 2004; Chételat et al., 2005). As for the cortical methods, the main regions in the medial temporal, middle and inferior lateral temporal, inferior parietal, and posterior cingulated cortices and with a lesser extent parietal, frontal, and lateral occipital cortices, which is consistent with the previous group studies based on cortical thickness (Thompson et al., 2004; Lerch et al., 2005, 2008; McDonald et al., 2009).

In conclusion, we compared different automatic classification methods to assist in the early diagnosis of Alzheimer's disease using the ADNI database. Most of them classify AD and CN with

high accuracy. However, at the prodromal stage, their sensitivity was substantially lower. Combinations with other markers and/or more sophisticated prior knowledge seem necessary to be able to detect prodromal AD with high accuracy.

Acknowledgements

Data collection and sharing for this project was funded by the Alzheimer's Disease Neuroimaging Initiative (ADNI; Principal Investigator: Michael Weiner; NIH grant U01 AG024904). ADNI is funded by the National Institute on Aging, the National Institute of Biomedical Imaging and Bioengineering (NIBIB), and through generous contributions from the following: Pfizer Inc., Wyeth Research, Bristol-Myers Squibb, Eli Lilly and Company, GlaxoSmithKline, Merck & Co. Inc., AstraZeneca AB, Novartis Pharmaceuticals Corporation, Alzheimer's Association, Eisai Global Clinical Development, Elan Corporation plc, Forest Laboratories, and the Institute for the Study of Aging, with participation from the U.S. Food and Drug Administration. Industry partnerships are coordinated through the Foundation for the National Institutes of Health. The grantee organization is the Northern California Institute for Research and Education, and the study is coordinated by the Alzheimer's disease Cooperative Study at the University of California, San Diego. ADNI data are disseminated by the Laboratory of Neuro Imaging at the University of California, Los Angeles.

References

Ashburner, J., Friston, K.J., 2005. Unified segmentation. NeuroImage 26 (3), 839-51.

Ashburner, J., 2007. A fast diffeomorphic image registration algorithm. NeuroImage 38 (1), 95-113.

Bach, F., Lanckriet, G., Jordan, M.I., 2004. Multiple kernel learning, conic duality, and the SMO algorithm. In Proceedings of the 21st International Conference on Machine Learning, 41-8.

Bakkour, A., Morris, J.C., Dickerson, B.C., 2009. The cortical signature of prodromal AD: regional thinning predicts mild AD dementia. Neurology 72 (12), 1048-55.

Bergouignan, L., Chupin, M., Czechowska, Y., Kinkingnéhun, S., Lemogne, C., Le Bastard, G., Lepage, M., Garnero, L., Colliot, O., Fossati P., 2009. Can voxel based morphometry, manual segmentation and automated segmentation equally detect hippocampal volume differences in acute depression? NeuroImage 45 (1), 29-37.

Blennow, K., de Leon, M.J., Zetterberg, H., 2006. Alzheimer's disease. Lancet 368 (9533), 387-403.

Busatto, G.F., Garrido, G.E., Almeida, O.P., Castro, C.C., Camargo, C.H., Cid, C.G., Buchpiguel, C.A., Furuie, S., Bottino, C.M., 2003. A voxel-based morphometry study of temporal lobe gray matter reductions in Alzheimer's disease. Neurobiology of Aging 24 (2), 221-31.

Chang, C.-C., Lin C.-J., 2001. LIBSVM: a library for support vector machines. Software available at http://www.csie.ntu.edu.tw/~cjlin/libsvm.

Chételat, G., Baron, J.C., 2003. Early diagnosis of Alzheimer's disease: contribution of structural neuroimaging. NeuroImage 18 (2), 525-41.

Chételat, G., Landeau, B., Eustache, F., Mézenge, F., Viader, F., de la Sayette, V., Desgranges, B., Baron, J.C., 2005. Using voxel-based morphometry to map the structural changes associated with rapid conversion in MCI: a longitudinal MRI study. NeuroImage 27(4), 934-46.

Chupin, M., Mukuna-Bantumbakulu, A.R., Hasboun, D., Bardinet, E., Baillet, S., Kinkingnéhun, S., Lemieux, L., Dubois, B., Garnero, L., 2007. Automated segmentation of the hippocampus and the amygdala driven by competition and anatomical priors: Method and validation on healthy subjects

and patients with Alzheimer's disease. NeuroImage 34, 996-1019.

Chupin, M., Hammers, A., Liu, R.S., Colliot, O., Burdett, J., Bardinet, E., Duncan, J.S., Garnero, L., Lemieux, L., 2009a. Automatic segmentation of the hippocampus and the amygdala driven by hybrid constraints: method and validation. NeuroImage 46 (3), 749-61.

Chupin, M., Gérardin, E., Cuingnet, R., Boutet, C., Lemieux, L., Lehéricy, S., Benali, H., Garnero, L., Colliot, O., Alzheimer's Disease Neuroimaging Initiative, 2009b. Fully automatic hippocampus segmentation and classification in Alzheimer's disease and mild cognitive impairment applied on data from ADNI. Hippocampus 19 (6), 579-87.

Colliot, O., Chételat, G., Chupin, M., Desgranges, B., Magnin, B. Benali, H., Dubois, B., Garnero, L., Eustache, F., Lehéricy, S., 2008. Discrimination between Alzheimer disease, mild cognitive impairment, and normal aging by using automated segmentation of the hippocampus. Radiology 248 (1), 194-201.

Convit, A., De Leon, M.J., Tarshish, C., De Santi, S., Tsui, W., Rusinek, H., George, A., 1997. Specific hippocampal volume reductions in individuals at risk for Alzheimer's disease. Neurobiology of Aging 18 (2), 131-8.

Convit, A., de Asis, J., de Leon, M.J., Tarshish, C.Y., De Santi, S., Rusinek, H., 2000. Atrophy of the medial occipitotemporal, inferior, and middle temporal gyri in non-demented elderly predict decline to Alzheimer's disease. Neurobiology of Aging 21 (1), 19-26.

Dale, A.M., Fischl, B., Sereno, M.I., 1999. Cortical surface-based analysis. I. Segmentation and surface reconstruction. NeuroImage 9 (2), 179-94.

Davatzikos, C., Fan, Y., Wu, X., Shen, D., Resnick, S.M., 2008a. Detection of prodromal Alzheimer's disease via pattern classification of magnetic resonance imaging. Neurobiology of Aging 29 (4), 514-23.

Davatzikos, C., Resnick, S.M., Wu, X., Parmpi, P., Clark, C.M., 2008b. Individual patient diagnosis of AD and FTD via high-dimensional pattern classification of MRI. NeuroImage 41 (4), 1220-7.

Desikan, R.S., Segonne, F., Fischl, B., Quinn, B.T., Dickerson, B.C., Blacker, D., Buckner, R.L.,

52 Dale, A.M., Maguire, R.P., Hyman, B.T., Albert, M.S., Killiany, R.J., 2006. An automated labeling
53 system for subdividing the human cerebral cortex on MRI scans into gyral based regions of interest.
54 NeuroImage 31 (3), 968-80.
55 Desikan, R.S., Cabral, H.J., Hess, C.P., Dillon, W.P., Glastonbury, C.M., Weiner, M.W.,
56 Schmansky, N.J., Greve, D.N., Salat, D.H., Buckner, R.L., Fischl, B. and Alzheimer's Disease
57 Neuroimaging Initiative, 2009. Automated MRI measures identify individuals with mild cognitive
58 impairment and Alzheimer's disease. Brain 132 (8), 2048-57.
59 Dickerson, B.C., Bakkour, A., Salat, D.H., Feczko, E., Pacheco, J., Greve, D.N., Grodstein, F.,
60 Wright, C.I., Blacker, D., Rosas, H.D., Sperling, R.A., Atri, A., Growdon, J.H., Hyman, B.T.,
61 Morris, J.C., Fischl, B., Buckner, R.L., 2009. The cortical signature of Alzheimer's disease:
62 regionally specific cortical thinning relates to symptom severity in very mild to mild AD dementia
63 and is detectable in asymptomatic amyloid-positive individuals. Cerebral Cortex 19 (3), 497-510.
64 Dubois B., Albert M.L., 2004. Amnestic MCI or prodromal Alzheimer's disease? The Lancet
65 Neurology 3 (4), 246-48.
66 Dubois B., Feldman H.H., Jacova C., DeKosky S.T., Barberger-Gateau P., Cummings J., Delacourte
67 A., Galasko D., Gauthier S., Jicha G., Meguro K., O'Brien J., Pasquier F., Robert P., Rossor M.,
68 Salloway S., Stern Y., Visser P.J., Scheltens P., 2007. Research criteria for the diagnosis of
69 Alzheimer's disease: revising the NINCDS-ADRDA criteria. The Lancet Neurology 6 (8), 734-46.
70 Fan, Y., Shen, D., Davatzikos, C., 2005. Classification of structural images via high-dimensional
71 image warping, robust feature extraction, and SVM. In Proceedings of the 8th International
72 Conference on Medical Image Computing and Computer-Assisted Intervention 8 (Pt 1), 1-8.
73 Fan, Y., Shen, D., Gur, R.C., Davatzikosa, C., 2007. COMPARE: classification of morphological
74 patterns using adaptive regional elements. IEEE Transactions on Medical Imaging 26 (1), 93-105.
75 Fan, Y., Batmanghelich, N., Clark, C.M., Davatzikos, C., and the Alzheimer's Disease
76 Neuroimaging Initiative, 2008a. Spatial patterns of brain atrophy in MCI patients, identified via
77 high-dimensional pattern classification, predict subsequent cognitive decline. NeuroImage 39 (4),

1731-43.

Fan, Y., Resnick, S.M., Wu, X., Davatzikos, C., 2008b. Structural and functional biomarkers of prodromal Alzheimer's disease: a high-dimensional pattern classification study. NeuroImage 41 (2), 277-85.

Fischl, B., Sereno, M.I., Dale, A.M., 1999a. Cortical surface-based analysis. II: Inflation, flattening, and a surface based coordinate system. NeuroImage 9 (2), 195-207.

Fischl, B., Sereno, M.I., Tootell, R.B., Dale, A.M., 1999b. High-resolution intersubject averaging and a coordinate system for the cortical surface. Human Brain Mapping 8 (4), 272-84.

Fischl, B., Dale, A.M., 2000. Measuring the thickness of the human cerebral cortex from magnetic resonance images. Proceedings of the National Academy of Sciences of the United States of America 97, 11050-11055.

Fox, N.C., Schott, J.M., 2004. Imaging cerebral atrophy: normal ageing to Alzheimer’s disease. The Lancet 363 (9406), 392-4.

Gerardin, E., Chételat, G., Chupin, M., Cuingnet, R., Desgranges, B., Kim, H.-S., Niethammer, M., Dubois, B., Lehéricy, S., Garnero, L., Francis, E., Colliot, O., 2009. Multidimensional classification of hippocampal shape features discriminates Alzheimer's disease and mild cognitive impairment from normal aging. NeuroImage 47 (4), 1476-86.

Goldszal, A.F., Davatzikos, C., Pham, D.L., Yan, M.X., Bryan, R.N., Resnick, S.M., 1998. An image-processing system for qualitative and quantitative volumetric analysis of brain images. Journal of Computer Assisted Tomography 22 (5), 827-37.

Good, C.D., Johnsrude, I.S., Ashburner, J., Henson, R.N., Friston, K.J., Frackowiak, R.S., 2001. A voxel-based morphometric study of ageing in 465 normal adult human brains. NeuroImage 14 (1), 21-36.

Good, C.D., Scahill, R.I., Fox, N.C., Ashburner, J., Friston, K.J., Chan, D., Crum, W.R., Rossor, M.N., Frackowiak, R.S., 2002. Automatic differentiation of anatomical patterns in the human brain: validation with studies of degenerative dementias. NeuroImage 17 (1), 29-46.

Hajnal J.V., Hill D.L.G., Hawkes D.J., 2001. Medical image registration. New York: CRC Press.

Hinrichs, C., Singh, V., Mukherjee, L., Xu, G., Chung, M.K., Johnson, S.C., and the Alzheimer's Disease Neuroimaging Initiative, 2009. Spatially augmented LPboosting for AD classification with evaluations on the ADNI dataset. NeuroImage 48 (1), 138-49.

Hua, X., Lee, S., Yanovsky, I., Leow, A.D., Chou, Y.Y., Ho, A.J., Gutman, B., Toga, A.W., Jack, C.R.Jr, Bernstein, M.A., Reiman, E.M., Harvey, D.J., Kornak, J., Schuff, N., Alexander, G.E., Weiner, M.W., Thompson, P.M., and the Alzheimer's Disease Neuroimaging Initiative, 2009. Optimizing power to track brain degeneration in Alzheimer's disease and mild cognitive impairment with tensor-based morphometry: an ADNI study of 515 subjects. NeuroImage 48 (4), 668-81.

Jaccard P., 1901. Etude Comparative de la Distribution Florale dans une Portion des Alpes et du Jura, Bulletin de la Société vaudoise des Sciences Naturelles 37, 547-79.

Jack, C.R.Jr, Petersen, R.C., Xu, Y.C., Waring, S.C., O'Brien P.C., Tangalos, E.G., Smith, G.E., Ivnik, R.J., Kokmen, E., 1997. Medial temporal atrophy on MRI in normal aging and very mild Alzheimer's disease. Neurology 49 (3), 786-94.

Jack, C.R.Jr., Petersen, R.C., Xu, Y., O'Brien, P.C., Smith, G.E., Ivnik, R.J., Tangalos, E.G., Kokmen, E., 1998. Rate of medial temporal lobe atrophy in typical aging and Alzheimer's disease. Neurology 51(4), 993-9.

Jack, C.R.Jr, Bernstein, M.A., Fox, N.C., Thompson, P., Alexander, G., Harvey, D., Borowski, B., Britson, P.J., L Whitwell, J., Ward, C., Dale, A.M., Felmlee, J.P., Gunter, J.L., Hill, D.L., Killiany, R., Schuff, N., Fox-Bosetti, S., Lin, C., Studholme, C., DeCarli, C.S., Krueger, G., Ward, H.A., Metzger, G.J., Scott, K.T., Mallozzi, R., Blezek, D., Levy, J., Debbins, J.P., Fleisher, A.S., Albert M., Green, R., Bartzokis, G., Glover, G., Mugler, J., Weiner, M.W., 2008. The Alzheimer's Disease Neuroimaging Initiative (ADNI): MRI methods. Journal of Magnetic Resonance Imaging 27(4), 685-91.

Jagust, W., 2006. Positron emission tomography and magnetic resonance imaging in the diagnosis and prediction of dementia. Alzheimers Dementia 2, 36-42.

130 Jovicich J., Czanner S., Greve D., Haley E., van der Kouwe A., Gollub R., Kennedy D., Schmitt F.,
131 Brown G., MacFall J., Fischl B., Dale A.,2006. Reliability in multi-site structural MRI studies:
132 effects of gradient non-linearity correction on phantom and human data. NeuroImage, 30, 436-43.
133 Juottonen, K., Laakso, M.P., Insausti, R., Lehtovirta, M., Pitkänen, A., Partanen, K., Soininen, H.,
134 1998. Volumes of the entorhinal and perirhinal cortices in Alzheimer's disease. Neurobiology of
135 Aging 19 (1), 15-22.
136 Karas, G.B., Burton, E.J., Rombouts, S.A., van Schijndel, R.A., O'Brien, J.T., Scheltens, P.,
137 McKeith, I.G., Williams, D., Ballard, C., Barkhof, F., 2003. A comprehensive study of gray matter
138 loss in patients with Alzheimer's disease using optimized voxel-based morphometry. NeuroImage
139 18 (4), 895-907.
140 Karas, G.B., Scheltens, P., Rombouts, S.A., Visser, P.J., van Schijndel, R.A., Fox, N.C., Barkhof F.,
141 2004. Global and local gray matter loss in mild cognitive impairment and Alzheimer's disease.
142 NeuroImage 23 (2), 708-16.
143 Klein, A., Andersson, J., Ardekani, B.A., Ashburner, J., Avants, B., Chiang, M.C., Christensen,
144 G.E., Collins, D.L., Gee, J., Hellier, P., Song, J.H., Jenkinson, M., Lepage, C., Rueckert, D.,
145 Thompson, P., Vercauteren, T., Woods, R.P., Mann, J.J., Parsey, R.V., 2009. Evaluation of 14
146 nonlinear deformation algorithms applied to human brain MRI registration. NeuroImage 46 (3),
147 786-802.
148 Klöppel, S., Stonnington, C.M., Chu, C., Draganski, B., Scahill, R.I., Rohrer, J.D., Fox, N.C.,
149 Jack, C.R.Jr., Ashburner, J., Frackowiak, R.S.J., 2008. Automatic classification of MR scans in
150 Alzheimer's disease. Brain 131 (3), 681-9.
151 Laakso, M.P., Soininen, H., Partanen, K., Lehtovirta, M., Hallikainen, M., Hänninen, T., Helkala,
152 E.L., Vainio, P., Riekkinen, P.J.Sr., 1998. MRI of the hippocampus in Alzheimer's disease:
153 sensitivity, specificity, and analysis of the incorrectly classified subjects. Neurobiology of Aging 19
154 (1), 23-31.
155 Laakso, M.P., Frisoni, G.B., Könönen, M., Mikkonen, M., Beltramello, A., Geroldi, C., Bianchetti,

A., Trabucchi, M., Soininen, H., Aronen H.J., 2000. Hippocampus and entorhinal cortex in frontotemporal dementia and Alzheimer's disease: a morphometric MRI study. Biol Psychiatry 47 (12), 1056-63.

Lanckriet, G.R.G., De Bie, T., Cristianini, N., Jordan, M.I., Noble, W.S., 2004. A statistical framework for genomic data fusion. Bioinformatics 20 (16), 2626-35.

Lao Z., Shen D., Xue Z., Karacali B., Resnick S.M., Davatzikos C., 2004. Morphological classification of brains via high-dimensional shape transformations and machine learning methods. NeuroImage 21 (1), 46-57.

Lerch, J.P., Pruessner, J.C., Zijdenbos, A., Hampel, H., Teipel, S.J., Evans, A.C., 2005. Focal decline of cortical thickness in Alzheimer's disease identified by computational neuroanatomy. Cerebral Cortex 15 (7), 995-1001.

Lerch, J.P., Pruessner, J., Zijdenbos, A.P., Collins, D.L., Teipel, S.J., Hampel, H., Evans, A.C., 2008. Automated cortical thickness measurements from MRI can accurately separate Alzheimer's patients from normal elderly controls. Neurobiology of Aging 29 (1), 23-30.

Levy-Cooperman, N., Ramirez, J., Lobaugh, N.J., Black, S.E., 2008. Misclassified tissue volumes in Alzheimer disease patients with white matter hyperintensities: importance of lesion segmentation procedures for volumetric analysis. Stroke 39 (4), 1134-41.

Magnin, B., Mesrob, L., Kinkingnéhun, S., Pélégrini-Issac, M., Colliot, O., Sarazin, M., Dubois, B., Lehéricy, S., Benali, H., 2009. Support vector machine-based classification of Alzheimer's disease from whole-brain anatomical MRI. Neuroradiology 51 (2), 73-83.

Marcus, D.S., Wang, T.H., Parker, J., Csernansky, J.G., Morris, J.C., Buckner, R.L., 2007. Open Access Series of Imaging Studies (OASIS): cross-sectional MRI data in young, middle aged, nondemented, and demented older adults. Journal of Cognitive Neuroscience 19 (9), 1498-507.

McDonald, C.R., McEvoy, L.K., Gharapetian, L., Fennema-Notestine, C., Hagler, D.J.Jr., Holland D., Koyama, A., Brewer, J.B., Dale, A.M., and the Alzheimer's Disease Neuroimaging Initiative, 2009. Regional rates of neocortical atrophy from normal aging to early Alzheimer disease.

182 Neurology 73 (6), 457-65.
183 McKhann G., Drachman D., Folstein M., Katzman R., Price D., Stadlan E.M., 1984. Clinical
184 diagnosis of Alzheimer's disease: report of the NINCDS-ADRDA Work Group under the auspices
185 of Department of Health and Human Services Task Force on Alzheimer's Disease. Neurology
186 34 (7), 939-44.
187 Misra C., Fan Y., Davatzikos C., 2009. Baseline and longitudinal patterns of brain atrophy in MCI
188 patients, and their use in prediction of short-term conversion to AD: Results from ADNI.
189 NeuroImage 44 (4), 1415-22.
190 Morris, J.C., 1993. The Clinical Dementia Rating (CDR): current version and scoring rules.
191 Neurology 43, 2412-14.
192 Mourao-Miranda J., Bokde A.L.W., Born C., Hampel H., Stetter M., 2005. Classifying brain states
193 and determining the discriminating activation patterns: Support Vector Machine on functional MRI
194 data. NeuroImage 28 (4) 980-95.
195 Narayana P.A., Brey W.W., Kulkarni M.V., Sievenpiper C.L., 1988. Compensation for surface coil
196 sensitivity variation in magnetic resonance imaging. Magnetic Resonance Imaging 6, 271-74.
197 Petersen, R.C., Smith, G.E., Waring, S.C., Ivnik, R.J., Tangalos, E.G., Kokmen, E., 1999. Mild
198 Cognitive Impairment: Clinical Characterization and Outcome. Archives of Neurology 56, 303-308.
199 Querbes, O., Aubry, F., Pariente, J., Lotterie, J.-A., Démonet, J.-F., Duret, V., Puel, M., Berry, I.,
200 Fort, J.-C., Celsis, P., and the Alzheimer's Disease Neuroimaging Initiative, 2009. Early diagnosis
201 of Alzheimer's disease using cortical thickness: impact of cognitive reserve. Brain 32 (8), 2036-47.
202 Rakotomamonjy, A., Bach, F.R., Canu, S., Grandvalet, Y., 2008. SimpleMKL. Journal of Machine
203 Learning Research 9, 2491-2521.
204 Rusinek, H., Endo, Y., De Santi, S., Frid, D., Tsui, W.H., Segal, S., Convit, A., de Leon, M.J., 2004.
205 Atrophy rate in medial temporal lobe during progression of Alzheimer disease. Neurology 63 (12),
206 2354-9.
207 Salat, D.H., Buckner, R.L., Snyder, A.Z., Greve, D.N., Desikan, R.S., Busa, E., Morris, J.C., Dale,

208 A.M., Fischl, B., 2004. Thinning of the cerebral cortex in aging. Cerebral Cortex 14(7), 721-30
209 Salat, D.H., Lee, S.Y., van der Kouwe, A.J., Greve, D.N., Fischl, B., Rosas, H.D., 2009. Age-
210 associated alterations in cortical gray and white matter signal intensity and gray to white matter
211 contrast. NeuroImage 48 (1), 21-8.
212 Schölkopf, B., Smola, A. J., 2001. Learning with Kernels. MIT Press.
213 Shattuck D.W., Sandor-Leahy S.R., Schaper K.A., Rottenberg D.A., Leahy R.M., 2001.
214 M. Resonance Image Tissue Classification Using a Partial Volume Model. NeuroImage 13 (5), 856-
215 76
216 Shawe-Taylor, J., Cristianini, N., 2000. Support Vector Machines and other kernel-based learning
217 methods. Cambridge University Press.
218 Shawe-Taylor, J., Cristianini, N., 2004. Kernel Methods for Pattern Analysis. Cambridge
219 University Press.
220 Sled, J.G., Zijdenbos, A.P., Evans, A.C., 1998. A nonparametric method for automatic correction of
221 intensity nonuniformity in MRI data. IEEE Transactions on Medical Imaging 17, 87-97.
222 Sonnenburg, S., Rätsch, G., Schäfer, C., Schölkopf, B., 2006. Large Scale Multiple Kernel
223 Learning. The Journal of Machine Learning Research archive 7, 1531-65.
224 Tapiola, T., Pennanen, C., Tapiola, M., Tervo, S., Kivipelto, M., Hänninen, T., Pihlajamäki, M.,
225 Laakso, M.P., Hallikainen, M., Hämäläinen, A., Vanhanen, M., Helkala, E.L., Vanninen, R.,
226 Nissinen, A., Rossi, R., Frisoni, G.B., Soininen, H., 2008. MRI of hippocampus and entorhinal
227 cortex in mild cognitive impairment: a follow-up study. Neurobiology of Aging 29 (1), 31-8.
228 Thompson, P.M., Mega, M.S., Woods, R.P., Zoumalan, C.I., Lindshield, C.J., Blanton, R.E.,
229 Moussai, J., Holmes, C.J., Cummings, J.L., Toga, A.W., 2001. Cortical change in Alzheimer's
230 disease detected with a disease-specific population-based brain atlas. Cerebral Cortex 11(1), 1-16.
231 Thompson, P.M., Hayashi, K.M., de Zubicaray, G., Janke, A.L., Rose, S.E., Semple, J., Herman,
232 D., Hong, M.S., Dittmer, S.S., Doddrell, D.M., Toga, A.W., 2003. Dynamics of gray matter loss in
233 Alzheimer's disease. The Journal of Neuroscience 23 (3), 994-1005.

234 Thompson, P.M., Hayashi, K.M., Sowell, E.R., Gogtay, N., Giedd, J.N., Rapoport, J.L., de
235 Zubicaray, G.I., Janke, A.L., Rose, S.E., Semple, J., Doddrell, D.M., Wang, Y., van Erp, T.G.,
236 Cannon, T.D., Toga, A.W., 2004. Mapping cortical change in Alzheimer's disease, brain
237 development, and schizophrenia. NeuroImage 23 (Suppl 1), S2-18.
238 Tzourio-Mazoyer, N., Landeau, B., Papathanassiou, D., Crivello, F., Etard, O., Delcroix, N.,
239 Mazoyer, B., Joliot, M., 2002. Automated anatomical labeling of activations in SPM using a
240 macroscopic anatomical parcellation of the MNI MRI single-subject brain. NeuroImage 15, 273-89.
241 Vapnik, V.N., 1995. The Nature of Statistical Learning Theory. Springer-Verlag New York Inc.
242 Vemuri, P., Gunter, J.L., Senjem, M.L., Whitwell, J.L., Kantarci, K., Knopman, D.S., Boeve, B.F.,
243 Petersen, R.C., Jack, C.R.Jr., 2008. Alzheimer's disease diagnosis in individual subjects using
244 structural MR images: validation studies. NeuroImage 39 (3), 1186-97.
245 Wechsler, D., 1987. Manual for the Wechsler Memory Scale-Revised. The Psychological
246 Corporation, San Antonio.
247 Whitwell, J.L., Przybelski, S.A., Weigand, S.D., Knopman, D.S., Boeve, B.F., Petersen, R.C., Jack,
248 C.R.Jr., 2007. Brain 130 (7), 1777-86.
249 Whitwell, J.L., Shiung, M.M., Przybelski, S.A., Weigand, S.D., Knopman, D.S., Boeve, B.F.,
250 Petersen, R.C., Jack, C.R.Jr., 2008. MRI patterns of atrophy associated with progression to AD in
251 amnestic mild cognitive impairment. Neurology 70 (7), 512-20.
252 Xu, Y., Jack, C.R.Jr, O'Brien, P.C., Kokmen, E., Smith, G.E., Ivnik, R.J., Boeve, B.F., Tangalos,
253 R.G., Petersen, R.C., 2000. Usefulness of MRI measures of entorhinal cortex versus hippocampus
254 in AD. Neurology 54 (9), 1760-7.
255 Yassa, M.A., Stark, C.E., 2009. A quantitative evaluation of cross-participant registration
256 techniques for MRI studies of the medial temporal lobe. NeuroImage 44 (2), 319-27.
257 Ye J., Chen K., Wu T., Li J., Zhao Z., Patel R., Bae M., Janardan R., Liu H., Alexander G., and
258 Reiman E., 2008. Heterogeneous data fusion for alzheimer's disease study. In Proceeding of the
259 14th ACM SIGKDD international Conference on Knowledge Discovery and Data Mining KDD '08,

1025-33.

Zekry, D., Hauw, J.J., Gold, G., 2002. Mixed dementia: epidemiology, diagnosis, and treatment. Journal of the American Geriatrics Society 8, 1431-8.

List of tables

Table 1. Demographic characteristics of the studied population (from the ADNI database). Values are indicated as mean ± standard-deviation [range].

Group	Diagnostic	Number	Age	Gender	MMS	# Centers
Whole set	CN	162	76.3 ± 5.4 [60 - 90]	76 M / 86 F	29.2 ± 1.0 [25 - 30]	40
	AD	137	76.0 ± 7.3 [55 - 91]	67 M / 70 F	23.2 ± 2.0 [18 - 27]	39
	MCIc	76	74.8 ± 7.4 [55 - 88]	43 M / 33 F	26.5 ± 1.9 [23 - 30]	30
	MCInc	134	74.5 ± 7.2 [58 - 88]	84 M / 50 F	27.2 ± 1.7 [24 - 30]	36
Training set	CN	81	76.1 ± 5.6 [60 - 89]	38 M / 43 F	29.2 ± 1.0 [25 - 30]	35
	AD	69	75.8 ± 7.5 [55 - 89]	34 M / 35 F	23.3 ± 1.9 [18 - 26]	32
	MCIc	39	74.7 ± 7.8 [55 - 88]	22 M / 17 F	26.0 ± 1.8 [23 - 30]	21
	MCInc	67	74.3 ± 7.3 [58 - 87]	42 M / 25 F	27.1 ± 1.8 [24 - 30]	30
Testing set	CN	81	76.5 ± 5.2 [63 - 90]	38 M / 43 F	29.2 ± 0.9 [26 - 30]	35
	AD	68	76.2 ± 7.2 [57 - 91]	33 M / 35 F	23.2 ± 2.1 [20 - 27]	33
	MCIc	37	74.9 ± 7.0 [57 - 87]	21 M / 16 F	26.9 ± 1.8 [24 - 30]	24
	MCInc	67	74.7 ± 7.3 [58 - 88]	42 M / 25 F	27.3 ± 1.7 [24 - 30]	31

Table 2. Summary of the approaches tested in this study.

FEATURES		SEGMENTATION REGISTRATION	TISSUES PROBABILITY MAPS	CLASSIFIER	METHOD #	METHOD'S NAME
Voxel – segmented tissue probability maps	*Direct*	DARTEL	GM	Linear SVM	*1.1.1 a*	*Voxel-Direct-D-gm*
			GM + WM + CSF	Linear SVM	*1.1.1 b*	*Voxel-Direct-D-all*
		SPM5	GM	Linear SVM	*1.1.2 a*	*Voxel-Direct-S-gm*
			GM + WM + CSF	Linear SVM	*1.1.2 b*	*Voxel-Direct-S-all*
	Direct VOI	DARTEL	GM	Linear SVM	*1.2.1 a*	*Voxel-Direct_VOI-D-gm*
			GM + WM + CSF	Linear SVM	*1.2.1 b*	*Voxel-Direct_VOI-D-all*
		SPM5	GM	Linear SVM	*1.2.2 a*	*Voxel-Direct_VOI-S-gm*
			GM + WM + CSF	Linear SVM	*1.2.2 b*	*Voxel-Direct_VOI-S-all*
	STAND-score	DARTEL	GM	Linear SVM	*1.3.1 a*	*Voxel-STAND-D-gm*
			GM + WM + CSF	Linear SVM	*1.3.1 b*	*Voxel-STAND-D-all*
		SPM5	GM	Linear SVM	*1.3.2 a*	*Voxel-STAND-S-gm*
			GM + WM + CSF	Linear SVM	*1.3.2 b*	*Voxel-STAND-S-all*
		SPM5 custom template	GM	Linear SVM	*1.3.3 a*	*Voxel-STAND-Sc-gm*
			GM + WM + CSF	Linear SVM	*1.3.3 b*	*Voxel-STAND-Sc-all*
	Atlas	DARTEL	GM	Linear SVM	*1.4.1 a*	*Voxel-Atlas-D-gm*
			GM + WM + CSF	Linear SVM	*1.4.1 b*	*Voxel-Atlas-D-all*
		SPM5	GM	Linear SVM	*1.4.2 a*	*Voxel-Atlas-S-gm*
			GM + WM + CSF	Linear SVM	*1.4.2 b*	*Voxel-Atlas-S-all*
	COMPARE	DARTEL	GM	Linear SVM	*1.5.1 a*	*Voxel-COMPARE-D-gm*
			GM + WM + CSF	Linear SVM	*1.5.1 b*	*Voxel-COMPARE-D-all*
		SPM5	GM	Gaussian SVM	*1.5.2 a*	*Voxel-COMPARE-S-gm*
			GM + WM + CSF	Gaussian SVM	*1.5.2 b*	*Voxel-COMPARE-S-all*
Cortical thickness	*Direct*	Freesurfer	-	Linear SVM	*2.1*	*Thickness-Direct*
	Atlas	Freesurfer	-	Linear SVM	*2.2*	*Thickness-Atlas*
	ROI	Freesurfer	-	Logistic Reg.	*2.3*	*Thickness-ROI*
Hippocampus	*Volume*	Freesurfer	-	Parzen	*3.1.1*	*Hippo-Volume-F*
	Volume	SACHA	-	Parzen	*3.1.2*	*Hippo-Volume-S*
	Shape	Freesurfer	-	Linear SVM	*3.2*	*Hippo-Shape*

Table 3. Contingency table for the McNemar test. ***a***: number of subjects correctly classified by both classifiers; ***b***: number of subjects correctly classified by classifier 1 but misclassified by classifier 2; ***c***: number of subjects misclassified by classifier 1 but correctly classified by classifier 2; ***d***: number of subjects misclassified by both classifiers.

	Classifier 2: correctly classified	Classifier 2: misclassified
Classifier 1: correctly classified	a	b
Classifier 1: misclassified	c	d

Table 4. Classification results CN *vs* AD.

		CN vs AD				
METHOD #	**METHOD'S NAME**	**SENSITIVITY**	**SPECIFICITY**	**PPV**	**NPV**	**MCNEMAR TEST**
1.1.1 a	*Voxel-Direct-D-gm*	81%	95%	93%	86%	p < 0.0001
1.1.1 b	*Voxel-Direct-D-all*	68%	98%	96%	78%	p < 0.0001
1.1.2 a	*Voxel-Direct-S-gm*	72%	89%	84%	79%	p < 0.0001
1.1.2 b	*Voxel-Direct-S-all*	65%	88%	81%	75%	p < 0.0001
1.2.1 a	*Voxel-Direct_VOI-D-gm*	71%	95%	92%	79%	p < 0.0001
1.2.1 b	*Voxel-Direct_VOI-D-all*	65%	95%	92%	76%	p < 0.0001
1.2.2 a	*Voxel-Direct_VOI-S-gm*	65%	91%	86%	76%	p < 0.0001
1.2.2 b	*Voxel-Direct_VOI-S-all*	59%	81%	73%	70%	p = 0.0012
1.3.1 a	*Voxel-STAND-D-gm*	69%	90%	85%	78%	p < 0.0001
1.3.1 b	*Voxel-STAND-D-all*	71%	91%	87%	79%	p < 0.0001
1.3.2 a	*Voxel-STAND-S-gm*	75%	91%	88%	81%	p < 0.0001
1.3.2 b	*Voxel-STAND-S-all*	75%	86%	82%	80%	p < 0.0001
1.3.3 a	*Voxel-STAND-Sc-gm*	72%	91%	88%	80%	p < 0.0001
1.3.3 b	*Voxel-STAND-Sc-all*	71%	91%	87%	79%	p < 0.0001
1.4.1 a	*Voxel-Atlas-D-gm*	78%	93%	90%	83%	p < 0.0001
1.4.1 b	*Voxel-Atlas-D-all*	81%	90%	87%	85%	p < 0.0001
1.4.2 a	*Voxel-Atlas-S-gm*	75%	93%	89%	82%	p < 0.0001
1.4.2 b	*Voxel-Atlas-S-all*	74%	93%	89%	81%	p < 0.0001
1.5.1 a	*Voxel-COMPARE-D-gm*	82%	89%	86%	86%	p < 0.0001
1.5.1 b	*Voxel-COMPARE-D-all*	69%	81%	76%	76%	p < 0.0001
1.5.2 a	*Voxel-COMPARE-S-gm*	66%	86%	80%	75%	p < 0.0001
1.5.2 b	*Voxel-COMPARE-S-all*	72%	91%	88%	80%	p < 0.0001
2.1	*Thickness-Direct*	74%	90%	86%	80%	p < 0.0001
2.2	*Thickness-Atlas*	79%	90%	87%	84%	p < 0.0001
2.3	*Thickness-ROI*	69%	94%	90%	78%	p < 0.0001
3.1.1	*Hippo-Volume-F*	63%	80%	73%	72%	p = 0.0007
3.1.2	*Hippo-Volume-S*	71%	77%	72%	76%	p = 0.0006
3.2	*Hippo-Shape*	69%	84%	78%	76%	p < 0.0001

291 **Table 5**. Classification results CN *vs* MCIc.

292

		CN vs MCIc				
METHOD #	**METHOD'S NAME**	**SENSITIVITY**	**SPECIFICITY**	**PPV**	**NPV**	**MCNEMAR TEST**
1.1.1 a	*Voxel-Direct-D-gm*	57%	96%	88%	83%	p = 0.00052
1.1.1 b	*Voxel-Direct-D-all*	49%	91%	72%	80%	p = 0.046
1.1.2 a	*Voxel-Direct-S-gm*	32%	96%	80%	76%	p = 0.039
1.1.2 b	*Voxel-Direct-S-all*	41%	94%	75%	78%	p = 0.044
1.2.1 a	*Voxel-Direct_VOI-D-gm*	54%	95%	83%	82%	p = 0.0022
1.2.1 b	*Voxel-Direct_VOI-D-all*	41%	96%	83%	78%	p = 0.0095
1.2.2 a	*Voxel-Direct_VOI-S-gm*	32%	88%	55%	74%	p = 0.83
1.2.2 b	*Voxel-Direct_VOI-S-all*	22%	99%	89%	73%	p = 0.046
1.3.1 a	*Voxel-STAND-D-gm*	73%	85%	69%	87%	p = 0.025
1.3.1 b	*Voxel-STAND-D-all*	65%	93%	80%	85%	p = 0.0019
1.3.2 a	*Voxel-STAND-S-gm*	59%	86%	67%	82%	p = 0.082
1.3.2 b	*Voxel-STAND-S-all*	49%	93%	75%	80%	p = 0.025
1.3.3 a	*Voxel-STAND-Sc-gm*	62%	85%	66%	83%	p = 0.091
1.3.3 b	*Voxel-STAND-Sc-all*	57%	90%	72%	82%	p = 0.026
1.4.1 a	*Voxel-Atlas-D-gm*	65%	80%	60%	83%	p = 0.27
1.4.1 b	*Voxel-Atlas-D-all*	54%	91%	74%	81%	p = 0.021
1.4.2 a	*Voxel-Atlas-S-gm*	68%	95%	86%	87%	p = 0.00020
1.4.2 b	*Voxel-Atlas-S-all*	59%	94%	81%	84%	p = 0.0021
1.5.1 a	*Voxel-COMPARE-D-gm*	49%	81%	55%	78%	p = 0.73
1.5.1 b	*Voxel-COMPARE-D-all*	51%	85%	61%	79%	p = 0.28
1.5.2 a	*Voxel-COMPARE-S-gm*	49%	78%	50%	77%	p = 0.87
1.5.2 b	*Voxel-COMPARE-S-all*	59%	78%	55%	81%	p = 0.64
2.1	*Thickness-Direct*	54%	96%	87%	82%	p = 0.00084
2.2	*Thickness-Atlas*	57%	93%	78%	82%	p = 0.0071
2.3	*Thickness-ROI*	65%	94%	83%	85%	p = 0.00083
3.1.1	*Hippo-Volume-F*	73%	74%	56%	86%	p = 0.47
3.1.2	*Hippo-Volume-S*	70%	73%	54%	84%	p = 0.67
3.2	*Hippo-Shape*	57%	88%	68%	82%	p = 0.072

293 PPV: positive predictive value; NPV: negative predictive value.
294
295

296

297 **Table 6**. Classification results MCInc *vs* MCIc.

		MCInc vs MCIc				
METHOD #	**METHOD'S NAME**	**SENSITIVITY**	**SPECIFICITY**	**PPV**	**NPV**	**MCNEMAR TEST**
1.1.1 a	*Voxel-Direct-D-gm*	0%	100%	-	64%	p = 1.0
1.1.1 b	*Voxel-Direct-D-all*	0%	100%	-	64%	p = 1.0
1.1.2 a	*Voxel-Direct-S-gm*	0%	100%	-	64%	p = 1.0
1.1.2 b	*Voxel-Direct-S-all*	0%	100%	-	64%	p = 1.0
1.2.1 a	*Voxel-Direct_VOI-D-gm*	43%	70%	44%	69%	p = 0.62
1.2.1 b	*Voxel-Direct_VOI-D-all*	0%	100%	-	64%	p = 1.0
1.2.2 a	*Voxel-Direct_VOI-S-gm*	0%	100%	-	64%	p = 1.0
1.2.2 b	*Voxel-Direct_VOI-S-all*	0%	100%	-	64%	p = 1.0
1.3.1 a	*Voxel-STAND-D-gm*	57%	78%	58%	76%	p = 0.40
1.3.1 b	*Voxel-STAND-D-all*	0%	100%	-	64%	p = 1.0
1.3.2 a	*Voxel-STAND-S-gm*	22%	91%	57%	68%	p = 0.79
1.3.2 b	*Voxel-STAND-S-all*	51%	79%	58%	75%	p = 0.49
1.3.3 a	*Voxel-STAND-Sc-gm*	35%	70%	39%	66%	p = 0.30
1.3.3 b	*Voxel-STAND-Sc-all*	41%	72%	44%	69%	p = 0.61
1.4.1 a	*Voxel-Atlas-D-gm*	0%	100%	-	64%	p = 1.0
1.4.1 b	*Voxel-Atlas-D-all*	0%	100%	-	64%	p = 1.0
1.4.2 a	*Voxel-Atlas-S-gm*	0%	100%	-	64%	p = 1.0
1.4.2 b	*Voxel-Atlas-S-all*	0%	100%	-	64%	p = 1.0
1.5.1 a	*Voxel-COMPARE-D-gm*	62%	67%	51%	76%	p = 1.0
1.5.1 b	*Voxel-COMPARE-D-all*	54%	78%	57%	75%	p = 0.50
1.5.2 a	*Voxel-COMPARE-S-gm*	32%	82%	50%	69%	p = 0.84
1.5.2 b	*Voxel-COMPARE-S-all*	51%	72%	50%	73%	p = 0.87
2.1	*Thickness-Direct*	32%	91%	67%	71%	p = 0.24
2.2	*Thickness-Atlas*	27%	85%	50%	68%	p = 0.82
2.3	*Thickness-ROI*	24%	82%	43%	66%	p = 0.66
3.1.1	*Hippo-Volume-F*	70%	61%	50%	79%	p = 0.89
3.1.2	*Hippo-Volume-S*	62%	69%	52%	77%	p = 0.88
3.2	*Hippo-Shape*	0%	100%	-	64%	p = 1.0

298 PPV: positive predictive value; NPV: negative predictive value.
299

300

Table 7. Order of magnitude of the computation time (i.e. minutes, hours, days, weeks) for each method for its three main phases: feature computation step (segmentation, registration), building of the classifier (including the grid search for the optimization of the hyperparameters and the learning of the classifier), classification of a new subject. The computations have been carried out with a processor running at 3.6 GHz with 2GB of RAM.

METHOD #	METHOD'S NAME	SEGMENTATION REGISTRATION	GRID SEARCH LEARNING	TESTING
1.1.1 a	*Voxel-Direct-D-gm*	Hour(s) per subject	Minute(s)	Minute(s)
1.1.1 b	*Voxel-Direct-D-all*	Hour(s) per subject	Minute(s)	Minute(s)
1.1.2 a	*Voxel-Direct-S-gm*	10 Minutes per subject	Minute(s)	Minute(s)
1.1.2 b	*Voxel-Direct-S-all*	10 Minutes per subject	Minute(s)	Minute(s)
1.2.1 a	*Voxel-Direct_VOI-D-gm*	Hour(s) per subject	Minute(s)	Minute(s)
1.2.1 b	*Voxel-Direct_VOI-D-all*	Hour(s) per subject	Minute(s)	Minute(s)
1.2.2 a	*Voxel-Direct_VOI-S-gm*	10 Minutes per subject	Minute(s)	Minute(s)
1.2.2 b	*Voxel-Direct_VOI-S-all*	10 Minutes per subject	Minute(s)	Minute(s)
1.3.1 a	*Voxel-STAND-D-gm*	Hour(s) per subject	Day(s)	Hour(s)
1.3.1 b	*Voxel-STAND-D-all*	Hour(s) per subject	Week(s)	Hour(s)
1.3.2 a	*Voxel-STAND-S-gm*	10 Minutes per subject	Day(s)	Hour(s)
1.3.2 b	*Voxel-STAND-S-all*	10 Minutes per subject	Week(s)	Hour(s)
1.3.3 a	*Voxel-STAND-Sc-gm*	20 Minutes per subject	Day(s)	Hour(s)
1.3.3 b	*Voxel-STAND-Sc-all*	20 Minutes per subject	Week(s)	Hour(s)
1.4.1 a	*Voxel-Atlas-D-gm*	Hour(s) per subject	Minute(s)	Minute(s)
1.4.1 b	*Voxel-Atlas-D-all*	Hour(s) per subject	Minute(s)	Minute(s)
1.4.2 a	*Voxel-Atlas-S-gm*	10 Minutes per subject	Minute(s)	Minute(s)
1.4.2 b	*Voxel-Atlas-S-all*	10 Minutes per subject	Minute(s)	Minute(s)
1.5.1 a	*Voxel-COMPARE-D-gm*	Hour(s) per subject	Week(s)	Hour(s)
1.5.1 b	*Voxel-COMPARE-D-all*	Hour(s) per subject	Week(s)	Hour(s)
1.5.2 a	*Voxel-COMPARE-S-gm*	10 Minutes per subject	Week(s)	Hour(s)
1.5.2 b	*Voxel-COMPARE-S-all*	10 Minutes per subject	Week(s)	Hour(s)
2.1	*Thickness-Direct*	Day(s) per subject	Minute(s)	Minute(s)
2.2	*Thickness-Atlas*	Day(s) per subject	Minute(s)	Minute(s)
2.3	*Thickness-ROI*	Day(s) per subject	Minute(s)	Seconds
3.1.1	*Hippo-Volume-F*	Day(s) per subject	Minute(s)	Seconds
3.1.2	*Hippo-Volume-S*	10 Minutes per subject	Minute(s)	Seconds
3.2	*Hippo-Shape*	Hour(s) per subject	Minute(s)	Seconds

List of tables for Supplementary Materials

Table S1. Optimal parameters values.

		CN vs AD	CN vs MCIc	MCInc vs MCIc
METHOD #	**METHOD'S NAME**	**OPTIMAL HYPERPARAMETERS**	**OPTIMAL HYPERPARAMETERS**	**OPTIMAL HYPERPARAMETERS**
1.1.1 a	*Voxel-Direct-D-gm*	Log10(C) = -3.5	Log10(C) = -3.5	Log10(C) = -5.0
1.1.1 b	*Voxel-Direct-D-all*	Log10(C) = -4.5	Log10(C) = -4.0	Log10(C) = -5.0
1.1.2 a	*Voxel-Direct-S-gm*	Log10(C) = -3.5	Log10(C) = -3.5	Log10(C) = -5.0
1.1.2 b	*Voxel-Direct-S-all*	Log10(C) = -4.0	Log10(C) = -4.0	Log10(C) = -5.0
1.2.1 a	*Voxel-Direct_VOI-D-gm*	Log10(C) = -1.5	Log10(C) = -1.0	Log10(C) = 0.0
1.2.1 b	*Voxel-Direct_VOI-D-all*	Log10(C) = -2.0	Log10(C) = -1.5	Log10(C) = -5.0
1.2.2 a	*Voxel-Direct_VOI-S-gm*	Log10(C) = -1.5	Log10(C) = -1.0	Log10(C) = -5.0
1.2.2 b	*Voxel-Direct_VOI-S-all*	Log10(C) = -1.0	Log10(C) = -2.0	Log10(C) = -5.0
1.3.1 a	*Voxel-STAND-D-gm*	Log10(C) = 0.5; t = 0.88	Log10(C) = -1.5; t = 0.80	Log10(C) = -2.0; t = 0.72
1.3.1 b	*Voxel-STAND-D-all*	Log10(C) = -2.0; t = 0.90	Log10(C) = -2.5; t = 0.64	Log10(C) = -5.0; t = 0.10
1.3.2 a	*Voxel-STAND-S-gm*	Log10(C) = -1.5; t = 0.84	Log10(C) = -2.0; t = 0.44	Log10(C) = -1.0; t = 0.90
1.3.2 b	*Voxel-STAND-S-all*	Log10(C) = -0.5; t = 0.90	Log10(C) = -3.5; t = 0.22	Log10(C) = -3.5; t = 0.34
1.3.3 a	*Voxel-STAND-Sc-gm*	Log10(C) = -3.0; t = 0.54	Log10(C) = -1.5; t = 0.54	Log10(C) = -1.5; t = 0.86
1.3.3 b	*Voxel-STAND-Sc-all*	Log10(C) = -4.0; t = 0.06	Log10(C) = -3.5; t = 0.18	Log10(C) = -2.0; t = 0.64
1.4.1 a	*Voxel-Atlas-D-gm*	Log10(C) = 0.5	Log10(C) = 1.5	Log10(C) = -5.0
1.4.1 b	*Voxel-Atlas-D-all*	Log10(C) = 0.5	Log10(C) = 0.5	Log10(C) = -5.0
1.4.2 a	*Voxel-Atlas-S-gm*	Log10(C) = 1.0	Log10(C) = 1.0	Log10(C) = -5.0
1.4.2 b	*Voxel-Atlas-S-all*	Log10(C) = 0.5	Log10(C) = 0.5	Log10(C) = -5.0
1.5.1 a	*Voxel-COMPARE-D-gm*	Log10(C) = 2.5 σ = 700; n = 20	Log10(C) = 1.5 σ = 500; n = 5	Log10(C) = 0.0 σ = 400; n = 4
1.5.1 b	*Voxel-COMPARE-D-all*	Log10(C) = 2.0 σ = 300; n = 16	Log10(C) = 2.0 σ = 300; n = 20	Log10(C) = 2.5 σ = 1000; n = 89
1.5.2 a	*Voxel-COMPARE-S-gm*	Log10(C) = 1.5 σ = 500; n = 6	Log10(C) = 1.0 σ = 200; n = 117	Log10(C) = 1.5 σ = 100; n = 128
1.5.2 b	*Voxel-COMPARE-S-all*	Log10(C) = 2.0 σ = 600; n = 98	Log10(C) = 2.0 σ = 1000; n = 5	Log10(C) = 1.0 σ = 100; n = 104
2.1	*Thickness-Direct*	Log10(C) = -5.0	Log10(C) = -5.0	Log10C = -5.0
2.2	*Thickness-Atlas*	Log10(C) = 0.0	Log10(C) = -0.5	Log10(C) = -0.5
2.3	*Thickness-ROI*	-	-	-
3.1.1	*Hippo-Volume-F*	-	-	-
3.1.2	*Hippo-Volume-S*	-	-	-
3.2	*Hippo-Shape*	Log10(C) = -1.5	Log10(C) = -1.0	Log10C = -5.0

Table S2. List of subjects from the ADNI database that were included in the study. This table lists the IDs of the subjects and the IDs of their T1 images (UID) as well as the series identifier (SID) for the CN training set.

CN: TRAINING SET				CN: TRAINING SET			
CENTER ID	SUBJECT ID	SID	UID	CENTER ID	SUBJECT ID	SID	UID
2	295	13408	45109	36	1023	24338	65105
2	1261	26574	62378	41	1002	23705	65221
2	1280	26453	60057	57	643	15782	34726
3	907	19728	52782	57 *	779 *	18109 *	80630 *
3	981	20753	52777	57	934	19971	34735
5	602	15966	32674	67	19	9539	45229
6	484	18837	65567	73	312	15079	39888
6	498	15857	67058	73	386	13746	49681
6	681	18451	92306	82	363	13017	39731
7	68	10356	35791	82	640	16562	49480
7	1222	25402	60004	94	489	14121	47292
11	2	9107	35470	94	711	16553	39139
11	5	9136	32247	98	171	11460	65753
11	16	9253	32307	98	896	19439	56032
11	21	9581	32342	99	533	14938	38786
11	22	9617	32394	109	1014	24818	63480
11	23	8868	32410	114	173	11594	96322
13	502	17232	51139	114	601	15201	39851
13	575	17859	51161	126	405	14635	38828
13	1035	21984	51166	126	506	15652	38855
14	519	14488	39648	126	605	15665	38705
14	520	14473	39661	126	680	16099	38927
14	558	15789	39684	127 *	260 *	12419 *	34385 *
20	883	19459	60674	127	622	15473	34453
20	899	19329	60628	128	863	19272	98876
20	1288	26890	60665	130	232	11928	39110
22	14	9271	59376	130	969	20385	39277
22	130	11089	59525	130	1200	25090	63753
23	61	10312	31103	131	123	10960	63785
23	963	19740	89418	131	319	12322	47985
24	985	21112	62716	131	441	13681	48030
24	1063	21525	63393	133	433	13952	39947
27 *	118 *	11796 *	34115 *	133	488	14150	107935
27	403	13717	34182	136	86	13191	66414
29	824	18139	96285	136	196	13253	40261
29	843	18909	66998	941	1194	25323	63848
33	920	19288	42482	941	1195	26180	63866
33	1098	22792	42833	941	1197	25332	66463
35	48	10257	45184	941	1202	25680	63875
36	672	17131	36939	941	1203	25671	63880
36	813	18252	36980				

*: images for which the cortical thickness extraction pipeline failed.
†: images for which the SPHARM computation pipeline failed.

Table S3. IDs of the subjects and the IDs of their T1 images (UID and SID) for the CN testing set.

CN: TESTING SET				CN: TESTING SET			
CENTER ID	SUBJECT ID	SID	UID	CENTER ID	SUBJECT ID	SID	UID
2	413	13893	45118	52	1250	25829	62241
2	559	14875	40675	52	1251	26231	62283
2	685	16309	40684	62	578	15035	50460
3	931	20051	53391	62	768	17527	50507
3	1021	21771	73507	62	1099	22713	50558
5	553	15527	32646	67	56	8723	35894
5	610	15727	32669	67	59	10517	35903
6	731	18321	90849	67	177	12187	34807
7	70	10950	36629	67	257	14730	34825
7	1206	25173	59982	73	89	11161	49676
11	8	9195	32265	73	311	15069	39869
13	1276	27641	62681	82	304	12557	95654
14	548	14921	39666	82	761	18119	39792
16	359	13000	96222	82	1256	26812	63157
16	538	17545	40773	94	526	14559	63469
20	97	10858	64047	94	692	17207	47296
22	66	10271	59447	94	1267	28217	80719
22	96	11006	59457	98	172	11812	65758
23	31	9785	69613	99	40	8920	34608
23	58	10335	30551	99	90	10835	35842
23	81	10813	31126	99	352	12992	34538
23	926	19390	31548	99	534	14009	34579
23	1190	24847	46418	109	876	19132	82595
23	1306	26604	46436	109	967	21137	55045
27	74	10605	34317	109	1013	22585	66150
27	120	11535	34333	114	166	11584	39811
29	845	18829	64868	114	416	13556	39837
29	866	18917	65612	127	259	12137	34363
33	516	14818	42309	127	684	16759	34459
33	734	16942	42435	130	886	19561	39173
33	741	17006	42451	131	436	14710	48021
33	923	19544	42510	131	1301	26899	63794
33	1016	21817	42773	133	493	14156	107944
33	1086	23547	42786	133	525	14991	39981
35	156	11391	39534	136	184	11974	40180
35	555	15332	39602	136	186	11774	40202
36	576	15156	36904	141	717	18413	98889
41	125	10883	35672	141	767	18337	47308
41	898	20306	34699	141	810	20274	47315
51	1123	24099	58044	141	1094	23294	47733
52	951	20352	64171				

*: images for which the cortical thickness extraction pipeline failed.

†: images for which the SPHARM computation pipeline failed.

Table S4. IDs of the subjects and the IDs of their T1 images (UID and SID) for the AD training set.

AD: TRAINING SET				AD: TRAINING SET			
CENTER ID	SUBJECT ID	SID	UID	CENTER ID	SUBJECT ID	SID	UID
2	816	18402	40732	67	812	19629	38727
2	938	19852	40981	67	828	18532	65717
2	955	20004	40755	67	1185	24635	63105
3	1059	22300	52817	67	1253	27558	55034
3	1257	27340	52791	73	565	15762	39920
5	814	18390	74592	82	1377	28495	63171
7	1248	25568	59951	94	1102	22905	63187
7	1304	26475	59911	94	1164	23871	67224
11	3	9127	32238	94	1397	31011	95663
11	10	8800	32275	94	1402	32102	66079
13	592	18419	79145	98	884	24183	56027
13	699	18366	62651	99	470	14222	34571
13	1161	24399	51486	99	492	14944	38771
14	356	12857	39630	99	1144	24218	102041
14	1095	23323	45741	109	777	18676	82577
22	129	11485	59485	114	374	13031	39818
23 (†)	78 (†)	10619 (†)	52000 (†)	114	979	21933	39860
23	84	10764	31207	126	606	17191	38910
23	139	11079	31304	126	1221	25457	48977
27	1081	25357	47169	127	844	19874	34472
29	836	18151	65014	128	1409	33787	69401
29	1184	25463	67211	128 *	1430 *	39199 *	79858 *
33	889	19296	51630	130	1290	26038	63767
35	341	12952	45217	130	1337	27584	63776
36	577	14974	36915	131	457	13976	92407
36	760	18264	38653	131	497	15315	48039
57	474	13990	34721	131	691	17266	48048
57	1371	28667	62999	133	1170	24674	89958
57	1373	28698	63009	136	299	13839	40313
57 (†)	1379 (†)	28761 (†)	63015 (†)	136	300	14136	40329
62	535	14699	50427	136	426	14581	40357
62	690	16924	50469	141	1024	22699	47749
62	730	17062	50488	141	1137	24301	48582
67	29	9904	38718	141	1152	24487	48591
67	76	10468	35912				

*: images for which the cortical thickness extraction pipeline failed.
†: images for which the SPHARM computation pipeline failed.

Table S5. IDs of the subjects and the IDs of their T1 images (UID and SID) for the AD testing set.

AD: TESTING SET				AD: TESTING SET			
CENTER ID	SUBJECT ID	SID	UID	CENTER ID	SUBJECT ID	SID	UID
2	1018	23128	40818	33	1281	26136	54781
5	221	11958	72129	33	1283	26144	54786
5	929	19669	74610	33	1285	26128	51589
5	1341	27673	60418	33	1308	26600	54753
6	547	16033	67316	36	759	18094	36970
6	653	16073	67325	36	1001	22691	38662
7	316	12583	36574	41	1368	27512	65249
7	1339	27414	56320	41	1391	29116	62934
11	53	10064	35487	41	1435	39186	79637
11	183	12000	32004	51	1296	26431	58024
13	996	22240	51184	53	1044	21256	64204
13	1205	25024	51543	62	793	18189	50525
14	328	12402	39621	67	110	11177	35934
16	991	21737	40795	82	1079	22650	49491
16	1263	27303	64623	94	1027	21207	49528
20	213	12386	60601	94	1090	23375	63177
22	7	9024	59367	98	149	11021	89430
22	219	12375	59535	99	372	13672	34550
22	543	14849	59544	109	1157	24711	66159
23	83	10568	31144	109	1192	25056	63504
23	93	10736	31254	114	228	11697	49736
23	916	19228	31534	126	784	19752	39013
23	1262	26314	62434	126 (†)	891 (†)	19386 (†)	39055 (†)
23	1289	26374	89939	127	431	14595	34444
24	1171	24659	63407	127	754	18515	80761
24	1307	27061	63416	127	1382	28261	66311
27	404	13866	34205	130	956	20667	39187
27	850	18554	48997	130	1201	25082	63758
27	1254	25764	47229	133	1055	22386	40029
27	1385	28133	47575	136	194	13178	40240
29	999	23248	64899	141	696	18373	82739
29	1056	22977	60742	141	790	18766	91254
33	724	17337	42401	141	852	19395	47745
33	733	16932	42426	141	853	18348	112293

*: images for which the cortical thickness extraction pipeline failed.

†: images for which the SPHARM computation pipeline failed.

Table S6. IDs of the subjects and the IDs of their T1 images (UID and SID) for the MCIc training set.

MCIc: TRAINING SET				MCIc: TRAINING SET			
CENTER ID	SUBJECT ID	SID	UID	CENTER ID	SUBJECT ID	SID	UID
2	954	19979	40745	33	906	19314	42469
2	1070	23120	40832	33	922	19341	42494
5	222	11754	54689	35	204	11661	39543
7	41	9994	35735	35	997	23184	62909
7	128	10936	36641	51	1331	29664	64153
7	344	12631	36580	52	952	20364	89953
11	856	19031	89409	52	1054	22955	62235
13	240	12308	51152	53	507	14483	80200
13	860	19237	51534	62	1299	26794	50585
22	750	17695	59553	67	243	12030	34820
22	1394	34317	68083	67	336	14023	34858
23	42	8852	31085	94	1015	21457	40764
23	388	13076	31438	94	1398	31771	63228
23	604	15182	31456	127	394	14603	34399
23	855	18561	31510	133	638	16608	67532
23	887	19087	31527	136	195	12523	40453
23	1247	25741	48858	141	982	22644	47704
27	461	15192	34232	941	1311	27408	97328
33	723	16845	42385	941	1363	28008	63898
33	725	17092	42410				

*: images for which the cortical thickness extraction pipeline failed.
†: images for which the SPHARM computation pipeline failed.

Table S7. IDs of the subjects and the IDs of their T1 images (UID and SID) for the MCIc testing set.

MCIc: TESTING SET				MCIc: TESTING SET			
CENTER ID	SUBJECT ID	SID	UID	CENTER ID	SUBJECT ID	SID	UID
2	729	16874	40709	57	941	19985	34748
5	572	15709	32659	57	1217	25854	62985
6	1130	23457	55973	67	45	10185	35889
7	249	11911	36531	67	77	11136	68121
11	241	12088	32021	94	434	13570	39124
11	861	19476	35514	98	269	11964	65258
11	1282	26225	62637	99	54	10329	35826
13	325	13524	54666	99	111	10933	35850
14	658	17481	39702	126	1077	23496	48881
23	30	9441	31632	127	1427	37933	91127
23	625	15820	31496	128	947	19859	69074
27	179	11781	34137	130	423	15030	39134
27	256	12357	34151	133	727	18620	66358
27	1213	25492	47224	133 (†)	913 (†)	24646 (†)	63820 (†)
27	1387	28123	67202	136	695	19019	70925
33	567	14572	42371	141	915	20504	48573
41	549	15488	39507	141	1244	26845	92647
41	1412	34022	72220	941	1295	26290	63889
41	1423	36902	72233				

*: images for which the cortical thickness extraction pipeline failed.
†: images for which the SPHARM computation pipeline failed.

Table S8. IDs of the subjects and the IDs of their T1 images (UID and SID) for the MCInc training set.

MCInc: TRAINING SET				MCInc: TRAINING SET			
CENTER ID	SUBJECT ID	SID	UID	CENTER ID	SUBJECT ID	SID	UID
3	1122	23542	52800	41	314	12492	34681
5	324	12599	32893	41	679	17077	40047
7	414	14826	36600	41	1010	23880	65231
11	326	12342	89391	41	1260	25806	65240
11	362	12678	89405	51	1072	22884	58012
11	1080	23159	35592	52	671	16062	64162
16	702	17341	40782	52	989	22476	64180
16	1028	22058	40800	52	1168	23688	65668
16	1138	24779	86046	53	621	15442	64190
22	1097	23337	59611	53	919	20422	65690
22	1351	28484	59616	57	464	14736	34708
23	126	11525	31272	57	1007	21339	47766
23	217	11731	31347	73	909	19716	75486
23	1046	22199	46397	94	1330	27038	63207
27	408	14231	37549	98	160	11224	65740
27	644	15630	34241	99	60	10478	35834
27	835	18760	35667	99	291	12065	34525
29	878	18986	64877	109	950	21165	97201
29	1038	22851	60733	114	378	12760	95689
29	1073	22828	65023	126	865	22295	39034
29	1215	25348	60747	126	1187	25143	48960
29	1218	25478	67390	127	112	11194	98858
33	511	15101	42241	127	1140	24278	63638
33	513	14673	42259	130	285	12462	39119
33	514	14663	42277	130	289	12111	39114
33	1279	26694	54758	130	449	22250	80931
33	1284	26686	54800	130	783	18023	39154
35	33	10396	45167	131	384	12790	48003
35	292	12408	39570	133	771	18575	92287
36	656	16286	36925	133	912	19884	40001
36	673	17157	36950	136	1227	26399	63839
36	748	17705	36960	141	697	18466	91236
36	869	21421	36994	141	851	19364	47871
36	976	23852	65092				

*: images for which the cortical thickness extraction pipeline failed.
†: images for which the SPHARM computation pipeline failed.

Table S9. IDs of the subjects and the IDs of their T1 images (UID and SID) for the MCInc testing set.

MCInc: TESTING SET				MCInc: TESTING SET			
CENTER ID	SUBJECT ID	SID	UID	CENTER ID	SUBJECT ID	SID	UID
2	782	17835	40718	62	1182	25166	50567
2	1155	24144	40846	73	746	23286	63123
3	908	32516	62590	82	1119	23733	63148
3	1074	23536	53396	94	531	14554	49667
5	448	14032	32877	94	921	19582	49511
5	546	15566	32683	94	1293	27865	64375
5	1224	25412	60407	94	1314	27488	63197
7	101	10679	36727	98	667	15980	89496
7	293	12193	36550	99	51	10325	35820
7	698	16403	36614	99	1034	21759	47954
13	1186	25689	62657	109	1114	24702	63490
14	169	11565	40859	109	1183	24718	66168
14	557	15094	39675	114	410	13289	39825
14	563	16079	39693	114	458	14111	39846
16	769	17720	48868	114	1103	23239	49758
22	4	9234	64632	114	1106	22859	49911
22	544	14679	64673	114	1118	23803	49769
22	961	20711	59602	126	708	16897	38945
23	331	12428	31374	126	709	17326	38965
23	376	12652	31385	127	393	13200	34394
27	116	11442	34326	127	925	21560	67267
27	307	13072	34160	127	1032	22259	63633
27	485	14208	37558	128	1043	22562	69092
27	1045	22174	47211	130	102	10746	39461
33	1116	22799	42845	130	505	17292	39144
33	1309	26195	51606	133	629	15915	40955
36	945	20971	37000	133	792	18306	66374
36	1135	24501	65110	133	1031	21552	40020
36	1240	26423	65119	136	107	11707	40446
41	282	13496	39487	136	429	15534	40388
41	598	15604	40038	136	579	15952	40411
51	1131	24089	62944	136	874	22234	40420
53	389	13550	65677	141	1052	22923	47723
57	839	19188	38671				

*: images for which the cortical thickness extraction pipeline failed.
†: images for which the SPHARM computation pipeline failed.

List of figures

Figure 1. Classification results for the different methods.

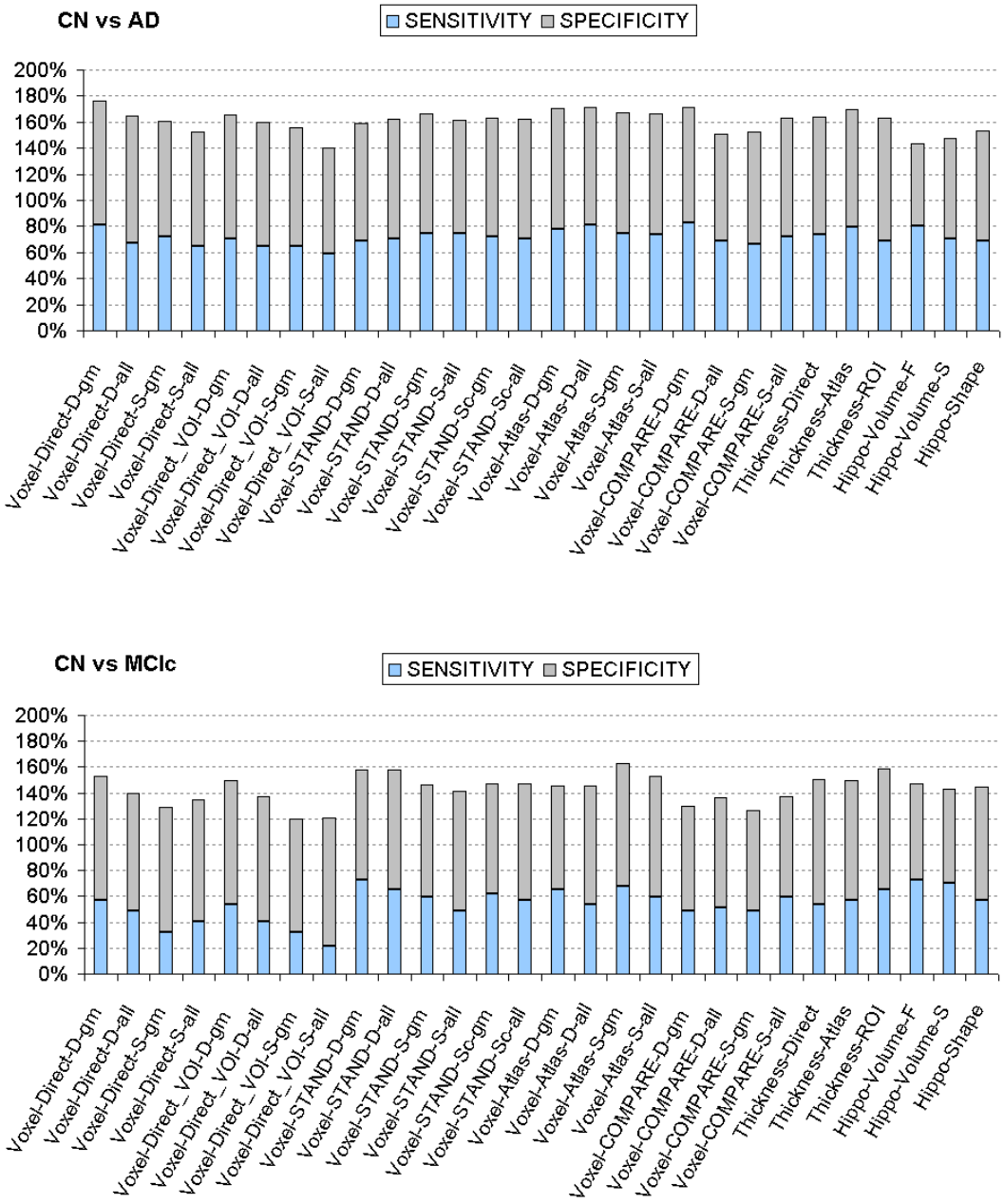

Figure 2. Impact of the preprocessing on the accuracy for CN *vs* AD. The sum of the sensitivity and specificity is considered. The front tip of an arrow indicates the results obtained with DARTEL whereas the back tip indicates the results obtained with SPM5 unified segmentation. The color of the arrow indicates the features used. Grey arrows correspond to the use of GM probability maps only whereas white arrows correspond to the use of GM, WM and CSF probability maps. The p-values obtained with the McNemar's chi square test assessed the difference between the results obtained with DARTEL and SPM5.

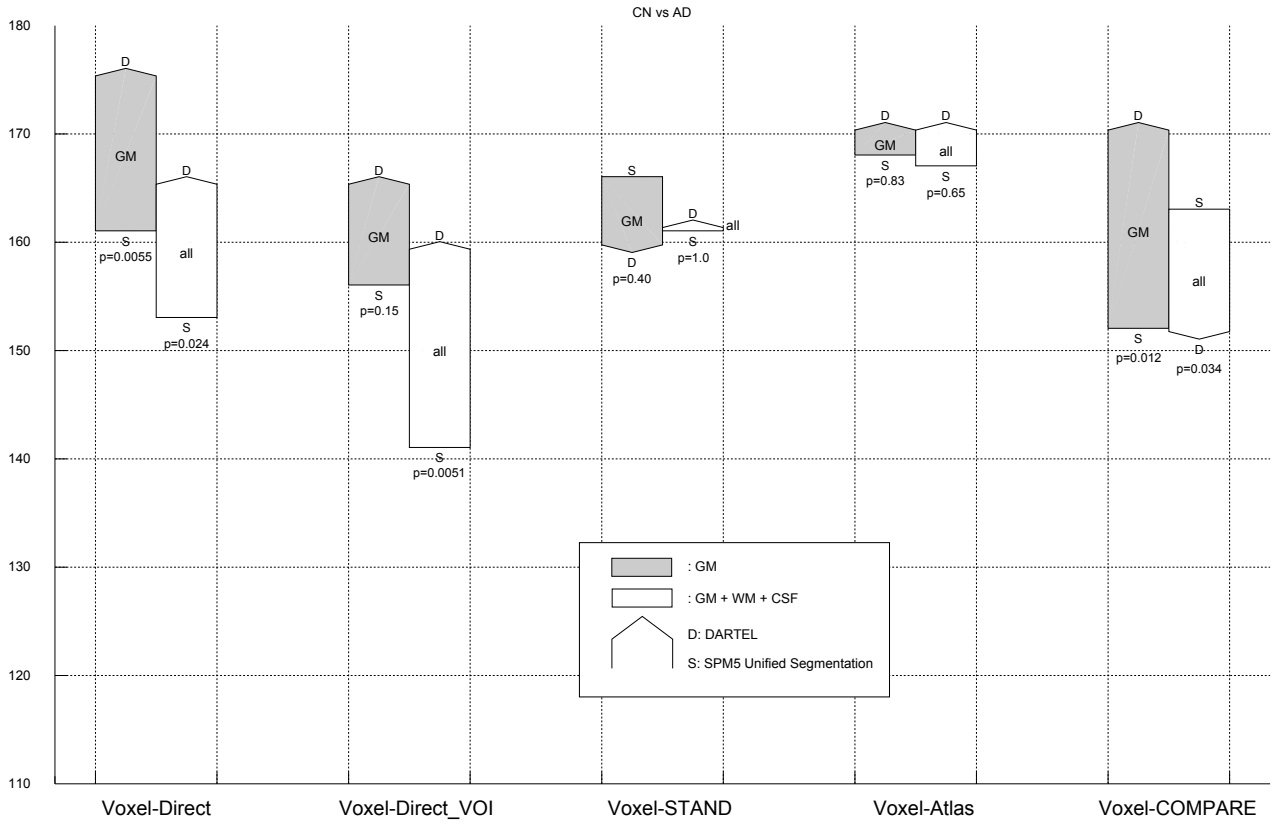

Figure 3. Impact of the preprocessing on the accuracy for CN *vs* MCIc. The sum of the sensitivity and specificity is considered. The front tip of an arrow indicates the results obtained with DARTEL whereas the back tip indicates the results obtained with SPM5 unified segmentation. The color of the arrow indicates the features used. Grey arrows correspond to the used of GM probability maps only whereas white arrows correspond to the use of GM, WM and CSF probability maps. The p-values obtained with the McNemar's chi square test assessed the difference between the results obtained with DARTEL and SPM5.

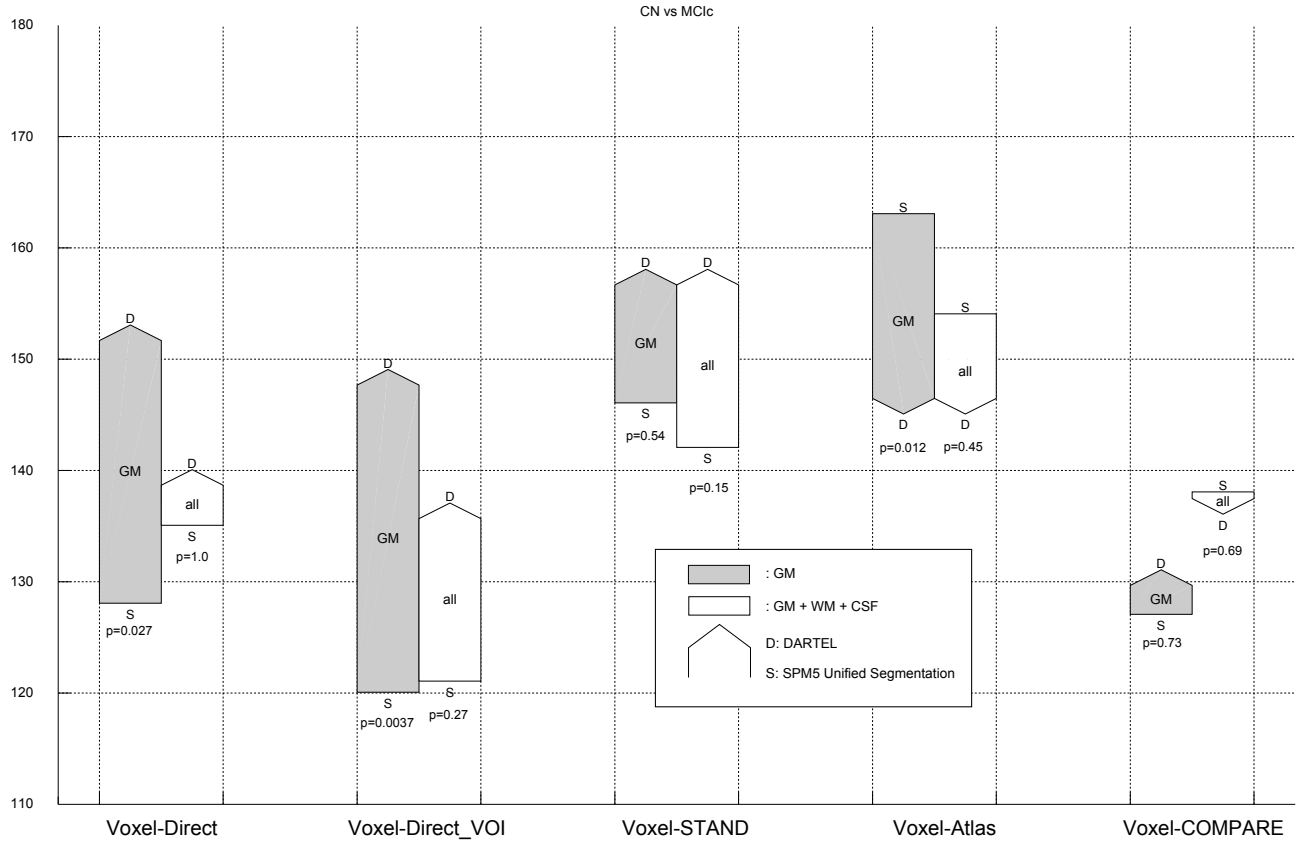

Figure 4. Optimal margin hyperplane in the CN vs AD experiments for *Voxel-Direct-D-gm* (a), *Voxel-Direct-D-all* (b-d), *Voxel-Direct-S-gm* (e), *Voxel-STAND-D-gm* (f) and *Voxel-Atlas-D-gm* (g). The figure displays the normalized vector orthogonal to the hyperplane superimposed on the tissue average probability maps. The coronal slices are equivalent to $y = 9mm$ in the MNI-space. For visualization purposes, only coefficients w_i greater than 0.15 in absolute value are displayed. For regions in warm colors, tissue atrophy increases the likelihood of classification into AD or MCIc. For regions in cool colors, it is the opposite.

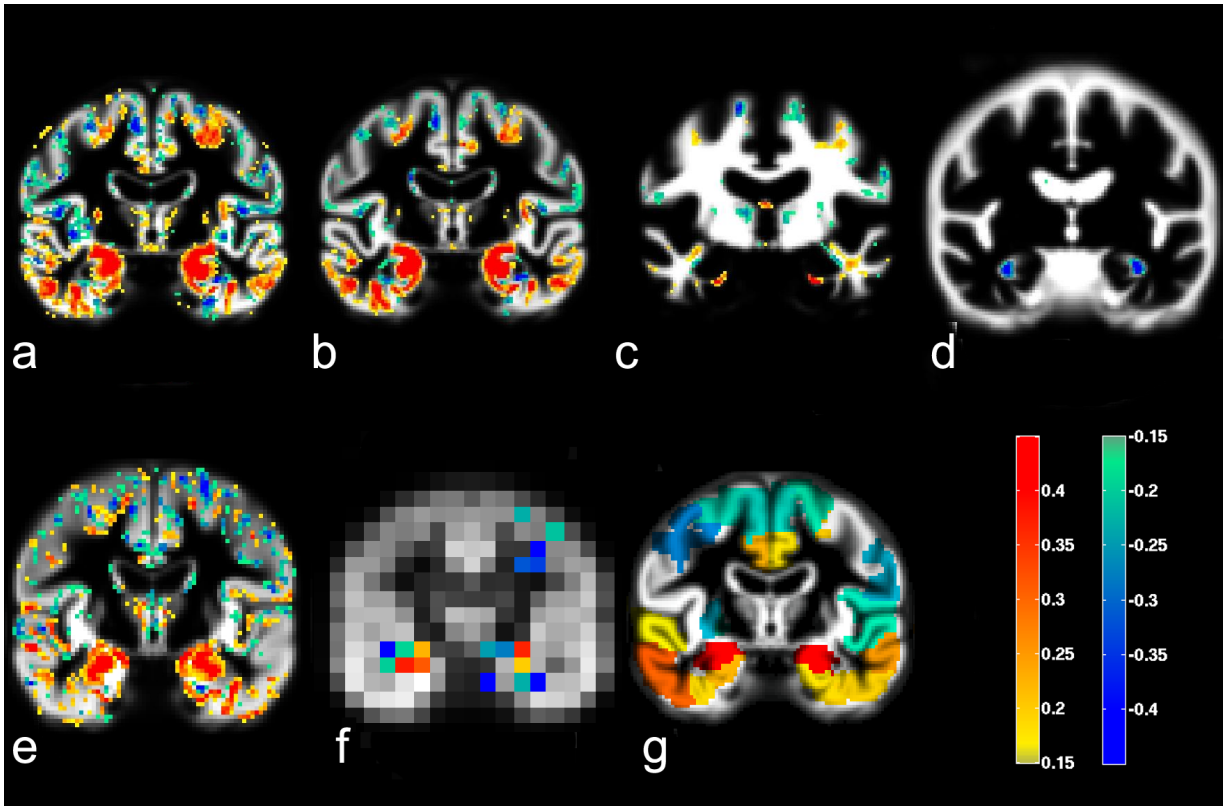

Figure 5. Optimal margin hyperplane in the CN *vs* MCIc experiments for *Voxel-Direct-D-gm* (a), *Voxel-Direct-D-all* (b-d), *Voxel-Direct-S-gm* (e), *Voxel-STAND-D-gm* (f) and *Voxel-Atlas-D-gm* (g) (please refer to Figure 4 for a complete description of the figure).

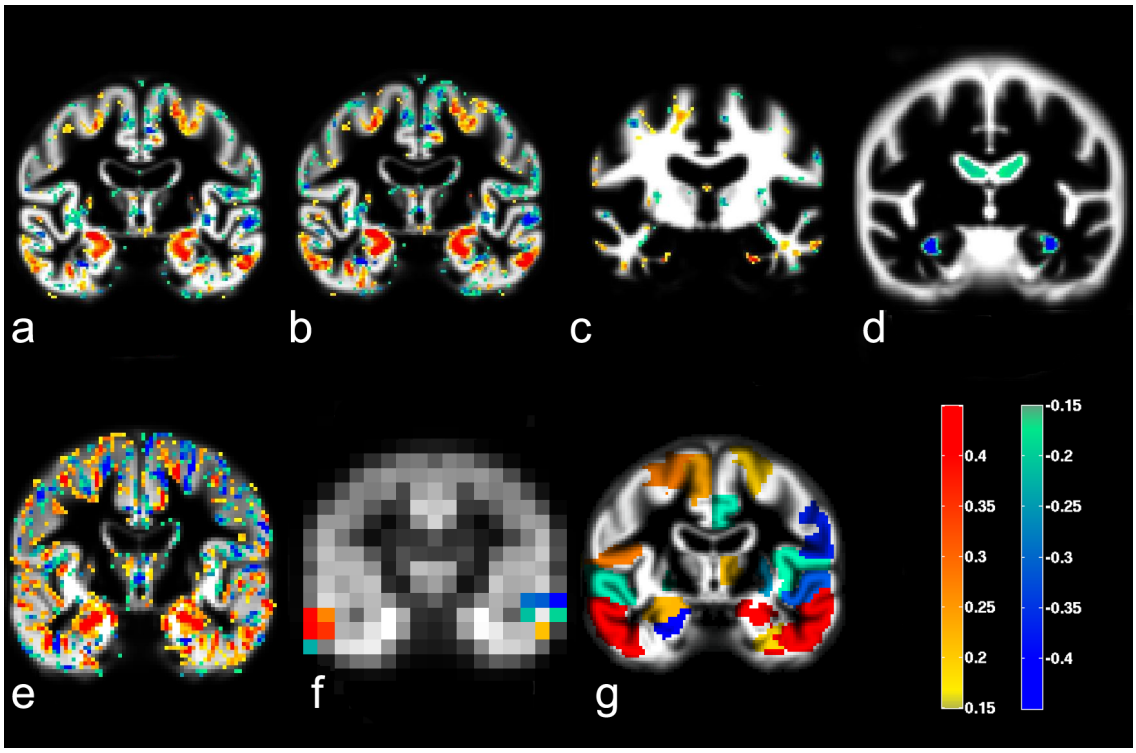

Figure 6. Optimal margin hyperplane for *Thickness-Atlas*. Upper rows: CN *vs* AD experiment. Lower rows: CN *vs* MCIc experiment.

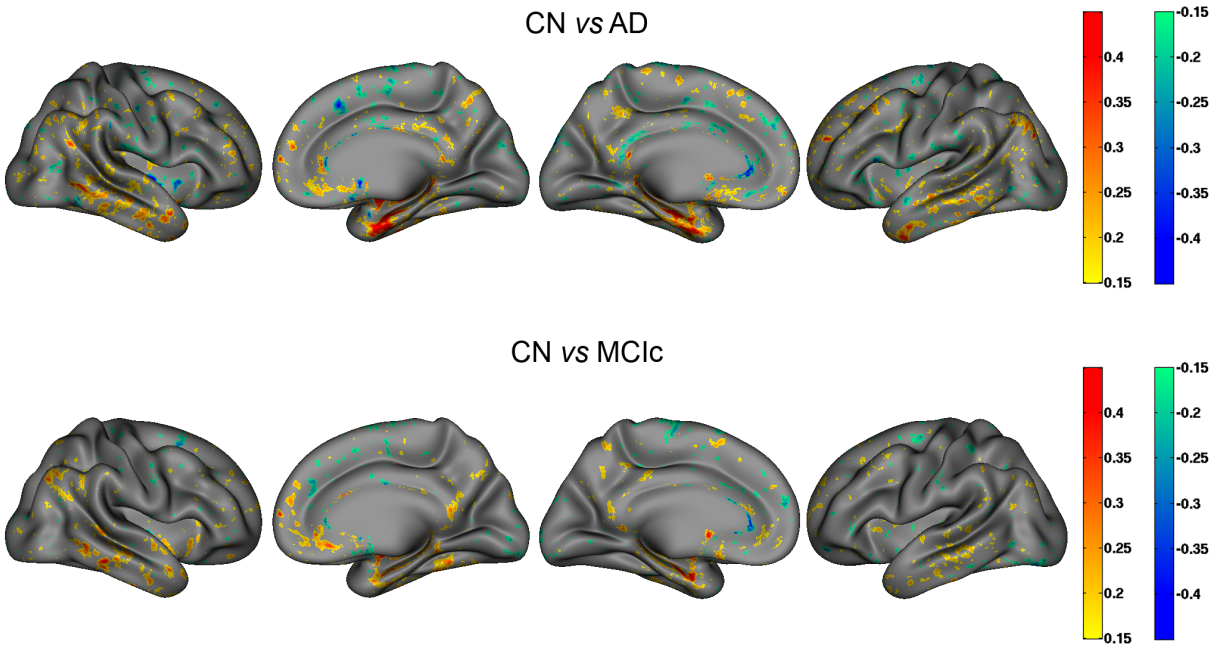

Figure 7. Optimal margin hyperplane for *Thickness-Direct*. Upper rows: CN *vs* AD experiment. Lower rows: CN *vs* MCIc experiment.

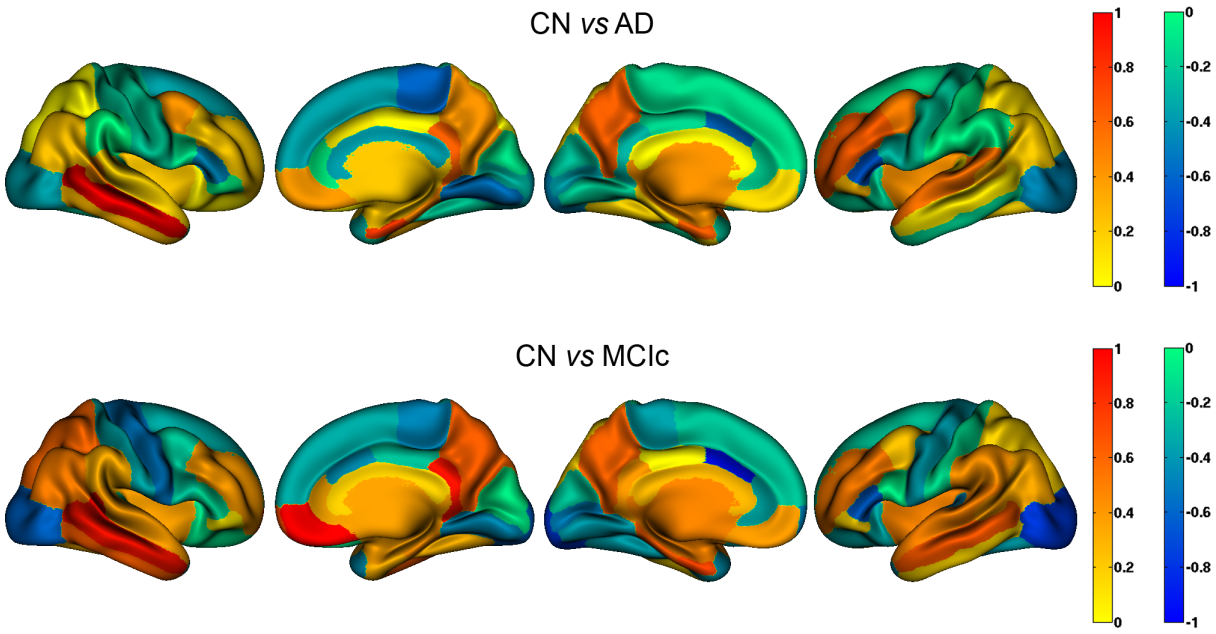

List of figures for Supplementary Materials

Figure S1. Jaccard index of similarity between the different classification methods for CN *vs* AD. The Jaccard index of two methods is the number of subjects correctly classified by both methods divided by the number of subjects correctly classified by at least one of the two methods.

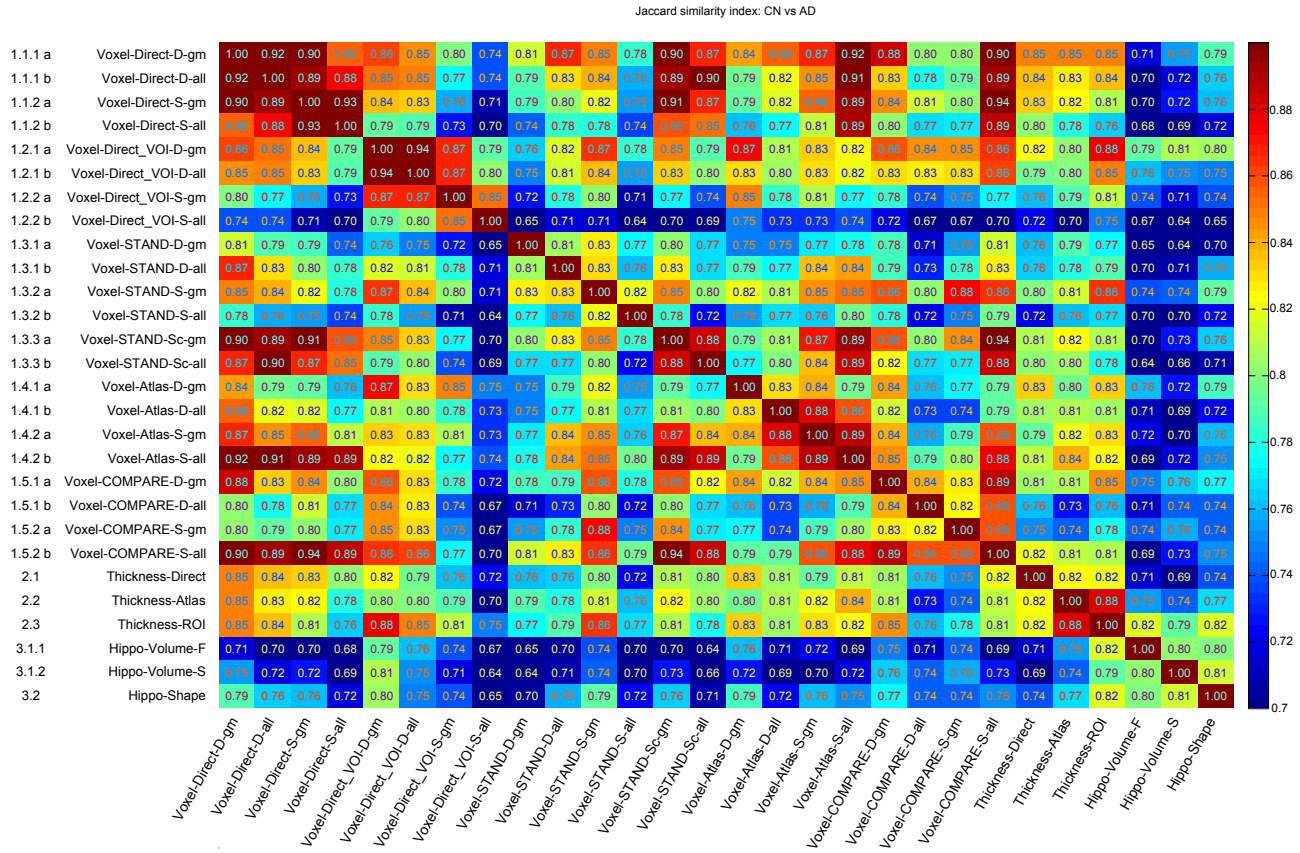

Figure S2. Jaccard index of similarity between the different classification methods for CN *vs* MCIc. The Jaccard index of two methods is the number of subjects correctly classified by both methods divided by the number of subjects correctly classified by at least one of the two methods.